PHOTOLUMINESCENT CONCENTRATOR BASED RECEPTIVE FIELDS

by

Paul Joseph Jungwirth
Bachelor of Science (Engineering Physics)
University of Saskatchewan, 1994

Thesis submitted in partial fulfillment of
the requirements for the degree of
Master of Applied Science

in the School
of
Engineering Science

SIMON FRASER UNIVERSITY
November 1996

Approval

Name: Paul Joseph Jungwirth

Degree: Master of Applied Science

Title of thesis: Photoluminescent Concentrator Based Receptive Fields

Examining Committee:

Chair: Dr. Marek Syrzycki
Professor, Engineering Science

_____

Dr. Glenn H. Chapman
Professor, Engineering Science
Examiner

_____

Dr. Andrew H. Rawicz
Professor, Engineering Science
Senior Supervisor

_____

Dr. M. Parameswaran
Associate Professor, Engineering Science
Supervisor

_____

Dr. Romuald Lakowski
Professor Emeritus
External Supervisor

Date Approved: November 15, 96

PARTIAL COPYRIGHT LICENSE

Title of Thesis/Project/Extended Essay

"Photoluminescent Concentrator Based Receptive Fields"

Author: _____
(signature)

Paul Jungwirth
(name)

October 4, 1996
(date)

ABSTRACT

This research describes a method of constructing an early vision system which makes use of photoluminescent concentrators. These are planar structures which can absorb light which is incident perpendicular to the plane, and then retransmit it along the plane. By coupling the light emitted around the perimeter of the structure to photodetectors, it is possible to create a large area detector while reducing the number of active optoelectronic transducers required. For most of this work, the photoluminescent concentrator used was patterned in the shape of a grid of intersecting lines which act as lightguides. In this way it is no longer a simple light detector, but acts as an imaging device since the location of the incident light, as well as its intensity is now measurable. This is the cornerstone of the receptive field system which was designed, built and tested. The receptive field system was designed as a precursor to an artificial retina based on some of the functionality of the human peripheral vision system.

The receptive field was interfaced to a computer in order to process the light signals collected. In this way it was possible to analyze the light pattern, and detect its size, shape, intensity gradient, and track its motion. Furthermore, by stacking a number of LCs directly over each other, with each one sensitive to a different portion of the visible spectrum, simple color processing was possible. This work serves as a large scale test bed and proof of concept for receptive fields which can now be easily fabricated on an integrated scale level which brings us one step closer to realizing a complete artificial vision system.

Acknowledgments

I would like to thank Dr. Eva Czyzewska, Scott Evenson, Dr. Romuald Lakowski, Dennis Michaelson, Brigitte Rabold, Dr. Andrew Rawicz, and Tomasz Wysokinski for their advice and technical contributions. I would also like to express my appreciation for my parents, family and friends and the support (financial and otherwise) they gave me during this work.

Table of Contents

List of Tables

List of Figures

Chapter 1
Introduction

1.1 Project Motivation

The goal of this work is to demonstrate a proof of concept for a simple imaging system using a photoluminescent concentrator as its primary sensing element. The final use of this device would be in an artificial vision system playing a similar role to the photoreceptors in the periphery of the human retina. As such, it was designed with the following characteristics. It would need to be an imaging device capable of functioning in normal daytime lighting conditions which could detect color, shape, size, motion, and intensity gradients, while not requiring a high degree of resolution, or significant post-processing.

1.2 Photoluminescent Concentrators

A photoluminescent concentrator (LC) is generally a planar structure composed of a transparent matrix in which is embedded some kind of photoluminescent material. When light falls on this type of structure, a portion of it is absorbed by the photoluminescent material, and then re-emitted at a shifted wavelength. By tailoring the structure geometry appropriately a large percentage of this re-emitted light will be trapped by total internal reflection (TIR) until it reaches the perimeter. Since the planar surface area illuminated is usually much larger than the structure's cross sectional area, the light escaping around the perimeter is highly concentrated (Batchelder, Zewail, and Cole 1979).

1.3 Receptive Fields

The concept of the receptive field was adapted from its biological counterpart. In the retina the photoreceptors (rods and cones) are connected directly and indirectly to several types of cells which provide feedforward and feedback functions, as well as serve to reduce the amount of information which flows from the detectors to the brain (Leibovic 1990, page 56). Thus a number of stimulated photoreceptors may contribute to the response of only a single neuron in the visual pathway. The area which they cover is known as a receptive field (Wandell 1995, page128), and in fact many of these receptive fields overlap (i.e.: a photoreceptor may 'belong' to a number of different receptive fields). There is also a center-surround mechanism which causes receptors on the perimeter of an illuminated receptive field to suppress the total response (Leibovic 1990, page 67). In this work a receptive field is essentially an area receiver which provides information convergence of incoming light signals. It consists of one or more LCs coupled to photodiodes, and the associated processing electronics. At present no center-surround mechanism or other feedback functions which occur in biological receptive fields are implemented in the system.

1.4 System Overview

The Receptive Field System (RFS) uses LC layers which were fabricated and patterned into shapes specifically designed for the purpose of collecting light falling on a large area and channeling it to a discrete set of photodiodes. The photoluminescent materials used were chosen for

their high efficiency, spectral absorption characteristics, and compatibility with the UV curable polymer used as the matrix. The photodiodes are connected to amplifiers and sample and hold circuits, which all work in parallel. The analog signals are then multiplexed and passed to a microprocessor which performs A/D conversions and other control functions. The digital information is then sent to a computer for software processing and for display purposes.

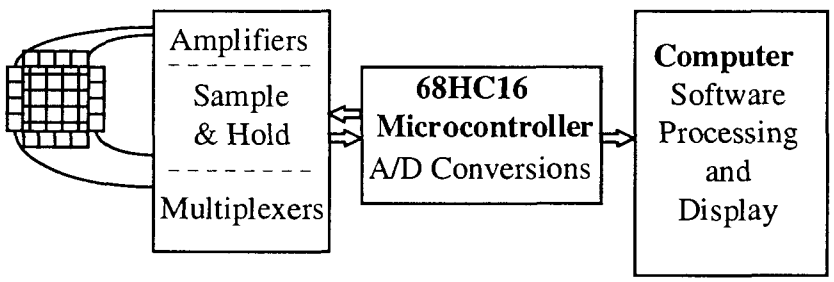

Figure 1.1 Receptive Field System Overview

The entire system is a macro-scale prototype which was built using discrete electronic components, and uses large (10 cm x 10 cm) LCs. This was done so that it could be developed in a relatively short time, tested, and then changes could be easily made if necessary. The final version of this system will be built on an integrated scale level using

microelectronics, and an LC approximately 1 cm^2 with a feature size of about 10μm. The development time for this technology tends to be longer, and changes cannot be easily made, so the large scale version was constructed as a test bed to work out any potential problems in advance.

In its present form the system could be easily applied for such tasks as laser positioning, or selective motion sensing devices. After conversion to the microscale version it could find uses in security systems, or in fact any other application where CCDs or cameras are used, but that expense and level of resolution is not justified. In an artificial vision system this receptive field chip could form a building block in creating the peripheral vision portion of an artificial retina.

Chapter 2
Photoluminescent Concentrators

2.1 Theory of Operation

As previously mentioned, photoluminescent concentrators are created by doping a planar optical matrix with some type of a photoluminescent material. The matrix is typically transparent and allows incident light to be absorbed by the photoluminescent centers which then re-emit the light at a shifted wavelength. The majority of this light is then trapped by total internal reflection and guided to the edges of the matrix according to the structure geometry.

2.1.1 Photoluminescent Materials

Materials are said to be photoluminescent if they can be excited by electromagnetic radiation and this leads to the emission of light (Berlman 1965, page 10). Typically, the emitted light is shifted to a longer wavelength compared to the exciting radiation in the process, and this is known as the Stokes Shift (Berlman 1965, page 2). The amount of Stokes shift is a characteristic of the particular photoluminescent material considered. For the materials used in this work, the absorption band is typically 50-100 nm wide, and the emission band is usually similar.

Other important parameters affecting the action of different photoluminescent materials are the following. They can absorb in different energy bands including ultraviolet, visible, and infrared regions,

and this can be chosen according to a particular application. The quantum efficiency of a particular photoluminescent material indicates the probability that an absorbed photon will cause emission, so usually a high value is desired. Finally, the time between a photon being absorbed by a photoluminescent center and one being emitted is called the decay time. However, this is generally on the order of a nanosecond (Schäfer 1977, page 29), which should be adequate for most applications.

2.1.2 Luminescent Concentrators

By combining photoluminescent materials with an appropriately designed transparent medium, a luminescent concentrator is created. In general it is a planar structure which accepts light incident on its surface, allowing it to be absorbed by the photoluminescent centers, traps the re-emitted light from these centers by TIR, and guides it to the perimeter of the structure. Due to the large difference between the planar area, and its cross sectional area, the light which reaches the edges is highly concentrated. The thickness of the LC could be a millimeter or more, down to a micron. Furthermore, the shape of the LC can be tailored for a particular application, so that the collected light can be coupled most efficiently to optoelectronic transducers, for example.

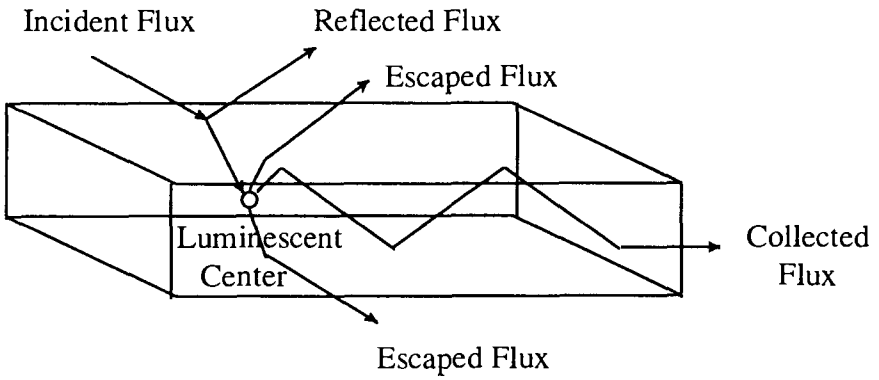

Figure 2.1 Luminescent Concentrator

The efficiency of the LC depends on a number of factors. In addition to considering the quantum efficiency of the particular photoluminescent material used, the LC must be doped with the appropriate concentration of this material. Also the thickness of the LC as well as the ratio between its planar area and cross sectional area are very important. Finally the transparent matrix itself can introduce various losses due to absorption, scattering, and reflection of the incident, and transmitted light.(Evenson and Rawicz, 1995) A slightly more detailed discussion of some design considerations and loss mechanisms involved in the construction of LCs will be given later.

2.2 Project Suitability

Some means was necessary to collect light falling on a relatively large area, and then convert it to electrical impulses for processing. There are a number of optoelectronic devices available which could have been chosen for this task, such as arrays of photodiodes or phototransistors or area CCDs. However, keeping the eventual goal of building an artificial retina in mind, there were a number of characteristics inherent to LCs which made them a better overall choice. Factors which needed to be considered were resolution, efficiency, sensitivity, color detection, power requirements, and adaptability.

Resolution and Color Processing

Area CCDs are available which have up to 1024x1024 rectangular photoelements which range from 9x9 to 18x18 microns (Texas Instruments, 1993). This would give images of excellent resolution, but it would not provide any information convergence as is desired for the periphery of the artificial retina. Furthermore, as a CCD cell has broad spectral sensitivity characteristics, it would not be able to perform color discrimination. Other area CCD sensors are available which utilize color filters can (Dillon et al 1976), but at the expense of reducing the spatial resolution. It works by having the photoelements dedicated to only detecting light in certain spectral ranges, similar to the cones in the human retina. An area array of photodiodes, or phototransistors might come close to giving the same resolution, but have the same problems with color processing and not be as sensitive.

Due to the unique nature of the photoluminescent concentrators, three or more could be stacked on top of each other with each layer absorbing and concentrating light of a specific wavelength band. In this manner there would be three dimensional selection and processing of the incoming light signals.

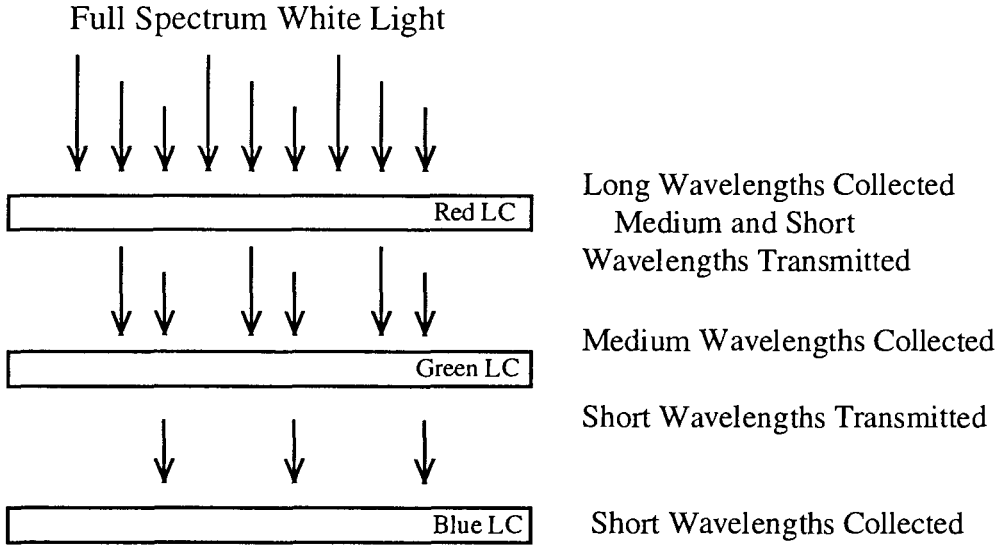

Figure 2.2 Stacked Color Processing Structure

As for the issue of resolution, luminescent concentrators can be constructed with line widths as small as 20 microns. They will still operate in a predictable manner as long as the dye concentrations, and other dimensions are adjusted accordingly (Evenson and Rawicz, 1995). The feature size is only limited by the IC fabrication equipment available, and it may be possible to create smaller functioning LCs in other

facilities. However, there is a tradeoff between thickness and the absorption efficiency, so the fabrication capabilities alone do not limit the reduction of feature size.

Efficiency, Sensitivity, and Power Requirements

The light collection efficiency of a CCD or a photodiode is very high compared to LCs. The former are nearly capable of detecting single photons, whereas even an ideal photoluminescent concentrator requires a much larger number of incident photons to produce a measurable signal at its edges. Modelling of an LC doped with Rhodamine 6G indicate optical efficiencies on the order of 10% (Evenson and Rawicz, 1995). One advantage to using LCs coupled to a linear array of photodiodes (or even linear CCD) is the fact that it will require fewer active elements than a CCD that could cover the same area of detection. This is due to the passive nature of luminescent concentrators. So an LC grid with NxN lines only requires 2N active elements as opposed to using a CCD with N^2 active photoelements for the same resolution. Furthermore, this results in a convergence of information which is necessary for the artificial eye project, and better realizes the receptive field concept.

Finally, it was decided that the system would only need to operate in normal daytime lighting conditions. LCs are sufficiently sensitive for that task. Certain things can be done to maximize their efficiency. For example, the top surface of the transparent matrix can have an anti-reflection coating applied to it to minimize reflection of incident light.

Also the LC can be mounted on top of a reflective surface called a back reflector. This increases the probability that the incident light is absorbed by the photoluminescent material by causing any flux which passes through unabsorbed to be reflected back through the LC a second time.

Adaptability

The final factor which had to be considered when choosing a particular type of technology for the optoelectronics necessary was its adaptability. While CCDs are excellent devices, they can not be easily modified, or integrated with application specific circuitry as easily. To try to replicate the receptive fields present in the retina may require the photodetectors to be overlapped in a similar fashion. This could not be done with CCDs, and to try to implement this with discretely fabricated photodiodes, which are also much less sensitive, would be very complicated. Photoluminescent concentrators could be overlapped, or interlinked easily, and even modifying their geometry would be a simple matter and not have to adversely affect their performance.

2.3 Macro Scale Luminescent Concentrators

2.3.1 Layout

As with most thin film devices, the planar geometry of an LC is only limited by the patterning resolution, and the imagination of the designer. A pattern which covered a large area was desired, but it had to be able to

interface with a number of discrete photodetectors. Earlier work with these LCs lead to the following basic layout for an ILCP (Evenson and Rawicz 1995).

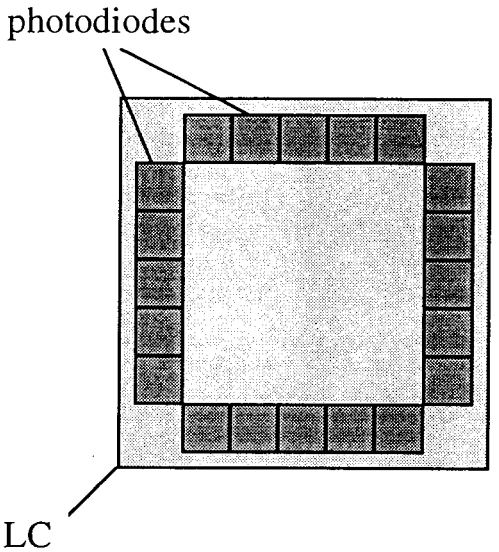

Figure 2.3 Simple Luminescent Concentrator

This scheme could be used for position detection of a point source focused on the LC since every photodiode would receive a signal but the photodiodes closest to the light spot would give the strongest signal due to less propagation losses. While this would be sufficient for a laser positioning system, it would be inadequate for to serve as an artificial retina. Figure 2.4 shows a couple of variations on the basic LC design which could yield more selective position information and in addition possibly allow for determination of the size and/or intensity of the incident light.

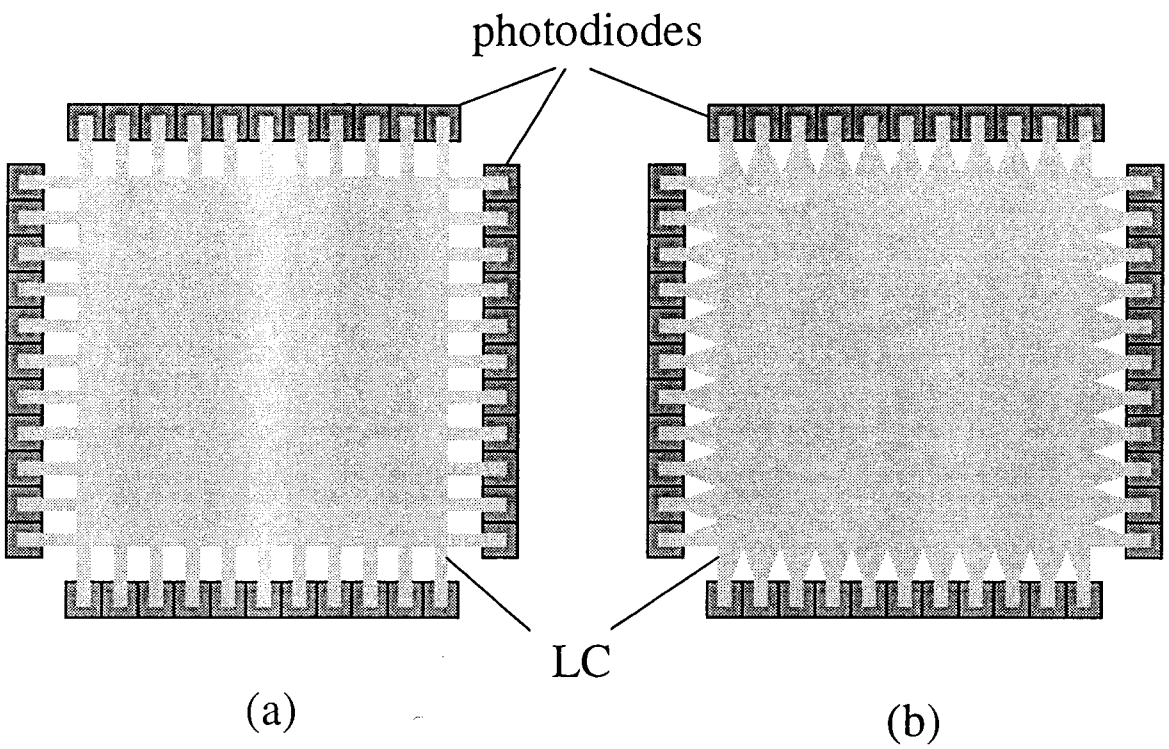

Figure 2.4 Selective Channel LCs

Going even further, it seemed reasonable to pattern the LC in the shape of a grid of intersecting lines (Figure 2.5). In this way, there would be automatic discretization of the incident light pattern allowing position, intensity, size, boundaries, and possibly the shape of the incident light pattern to be determined. Light signals theoretically would not be present at the ends of lines which were not directly illuminated by the incident light. This macro scale system was to be built using discrete components, so the line width (1 mm) and minimum line spacing in the grid (5 mm) was limited by the physical dimensions of the photodiodes used.

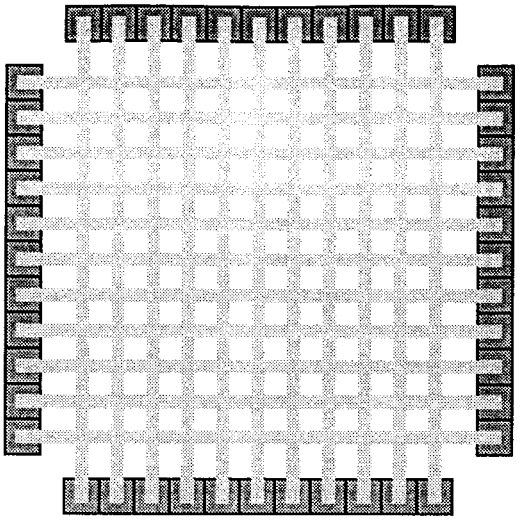

Figure 2.5 LC Grid

There are advantages and disadvantages to all of these designs. The first obviously yields the least amount of information. The third gives the most, but also does not take full advantage of the incoming light.

2.3.2 Optics

As briefly mentioned before, the collection and guiding of light by an LC is only possible due to total internal reflection, governed by the following relation. The light must strike the interface with $\theta_1 > \theta_c$ (see Figure 2.6) where the critical angle is defined by the following (Tamir 1988, page 10).

$$\sin \theta_c = n_1 / n_2 \qquad (2.1)$$

This is only possible of course if the refractive index of the LC (n_2) is greater than that of the material surrounding it (n_1, n_3).

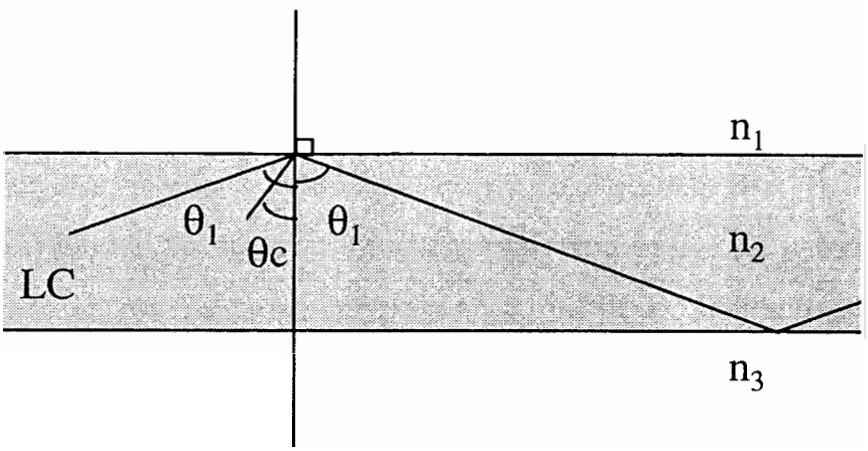

Figure 2.6 Total Internal Reflection

In a basic planar slab LC, the reflections only occur between the top and bottom surface of the structure. However, by changing the layout according to the designs in Figures 2.4 and 2.5, one must also consider the lateral reflections necessary to guide the light to the very ends of the channels. Therefore the waveguiding effects must be taken into account for these designs.

Going back to Figure 2.4(a), some light would reach all the photodiodes, but some light would be lost by escaping between the channels, thereby reducing the efficiency of the LC. In Figure 2.4(b) the angled structures leading to each channel help reduce those losses and increase the effective acceptance angle for each channel. The size of the angle used in this case will of course depend on the refractive indices of the LC and the surrounding material.

There are many forms of losses inherent in the transmission of light in an LC after absorption as it propagates toward the edges by total internal reflection. Critical cone losses, which occur due to the emitted

light striking the interface between the LC and air at angles smaller than the critical angle, are likely the most significant (Figure 2.7). This is especially true with the grid structure due to the intersection of the lines. In the figure, rays 1, 4, 6, and 7 all escape for this reason. Other types of propagation losses are absorption and scattering of the light by impurities or stress fractures in the matrix material, and self absorption by the photoluminescent material.

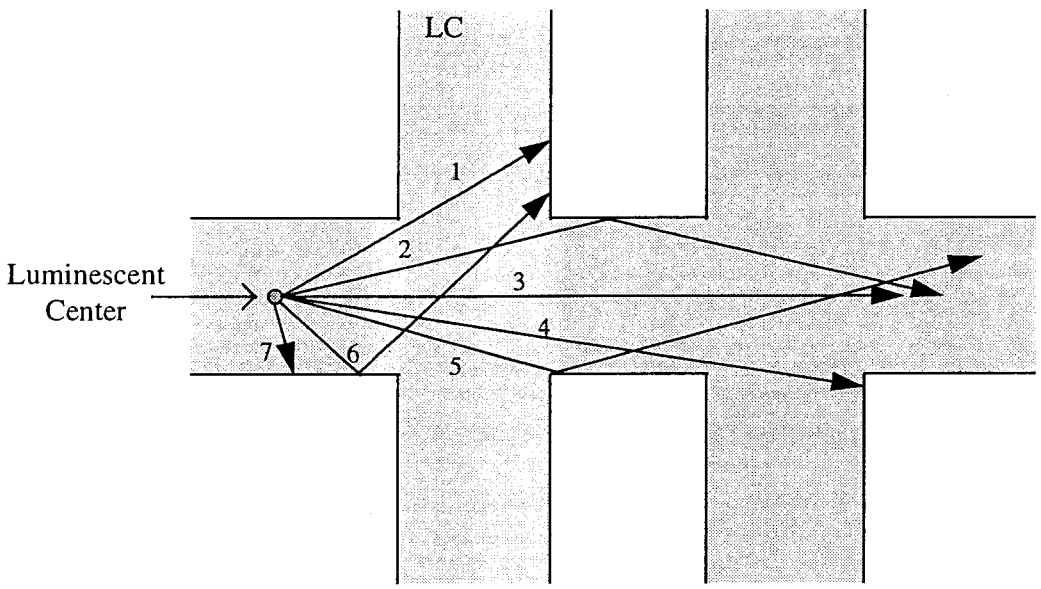

Figure 2.7 Critical Cone Losses

The other disadvantage the grid structure has is that its effective collection area is smaller than a planar LC of the same size due to the gaps between each gridline. Nevertheless, it was initially decided to proceed with the third design based on the assumption that the amount of information to be gained by using it outweighed the problem of higher critical cone losses, and reduced collection efficiency. However, later some experiments were performed with the design in Figure 2.4(b).

2.3.3 Materials

The grids were fabricated from a liquid polymer which could be cured using ultraviolet light, and patterned using standard photolithographic techniques. The exact processing steps and formulation of the polymer is included in Appendix A1. The grids are approximately 100 microns in thickness with a refractive index of 1.538 +/- 0.002 as measured with an Abbe Refractometer. Due to their large size and thickness they were designed as free standing structures which could be easily attached to the receptive field system and quickly replaced if necessary. In the microscale version however, they would be deposited onto the top surface of an ASIC chip containing all the photodiodes and processing electronics required.

The photoluminescent materials used were commercially available laser dyes with appropriate spectral responses and high quantum efficiencies. Several grids were fabricated, each doped with different dyes and of different concentrations. Below is a list of the types of dyes used, at what concentrations, their quantum efficiencies, and absorption and emission peaks.

Laser Dye	Absorption Peak (nm)	Bandwidth, FWHM (nm)	Emission Peak (nm)	Concentrations Used (wt. %)
Sulforhodamine 101	578	35	602	0.01, 0.1
Rhodamine 6G	530	30	556	0.001, 0.01, 0.1
Coumarin 6	458	70	505	0.001, 0.01, 0.1
Coumarin 151	382	n/a	480	0.01, 0.1

Table 2.1 Laser Dyes

Initially, only the grids with the last three dyes listed in the table were fabricated. These were tested to determine which of the concentrations for each particular dye would give the best conversion efficiency. As mentioned previously, if the concentration is too high, concentration quenching can occur which can cause a drastic loss of efficiency (Schäfer 1977, page 9). However, with too low a concentration, there is a lower probability of absorption of the incident light, and would need to be compensated for by increasing the thickness of the LC. They were tested by illuminating a 1 cm^2 area of the grid different distances from the perimeter, and measuring the output at the end of 2 lines of the grid using a Handheld Newport Powermeter. The responses for each type of doped grid with their dye concentrations specified are shown in the following graphs (Figures 2.8, 2.9, 2.10). Based on these, it was decided that the following concentrations were best for the various dyes: 0.01% Rhodamine 6G, 0.001% Coumarin 6, 0.1% Coumarin 151. Note however that this is only valid for LC grids of these dimensions. It may not be

possible to generalize and assume that these would be appropriate concentrations for the microscale grids due to the affect the structure geometry has on absorption probability. For this reason, a much more comprehensive test of the dyes for different concentrations was not performed.

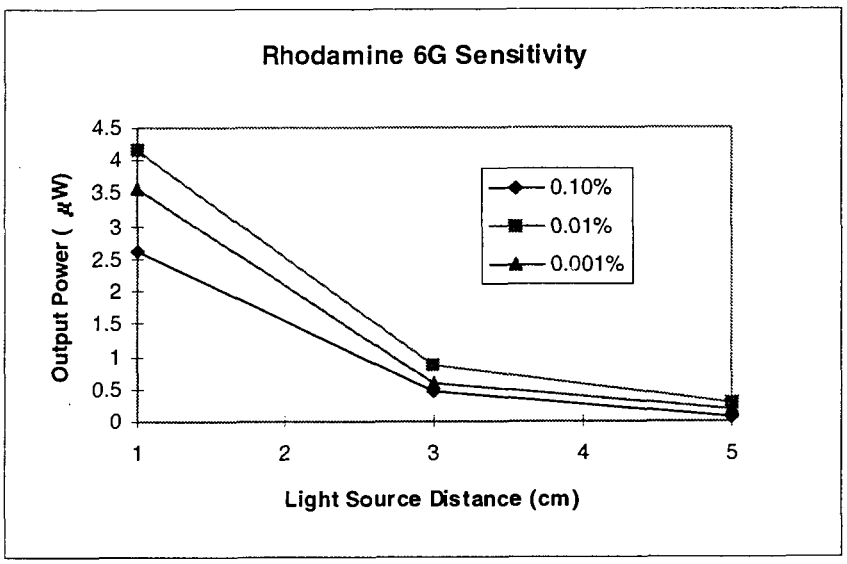

Figure 2.8 Rhodamine 6G Grid Responses

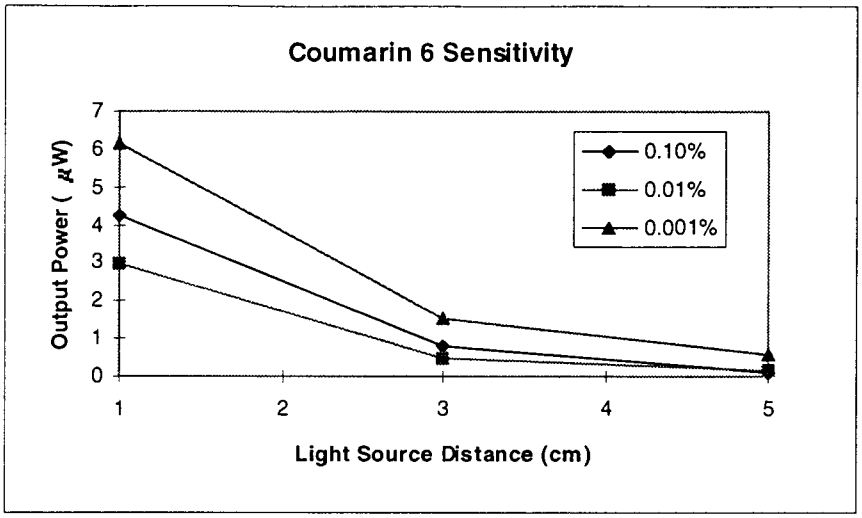

Figure 2.9 Coumarin 6 Grid Responses

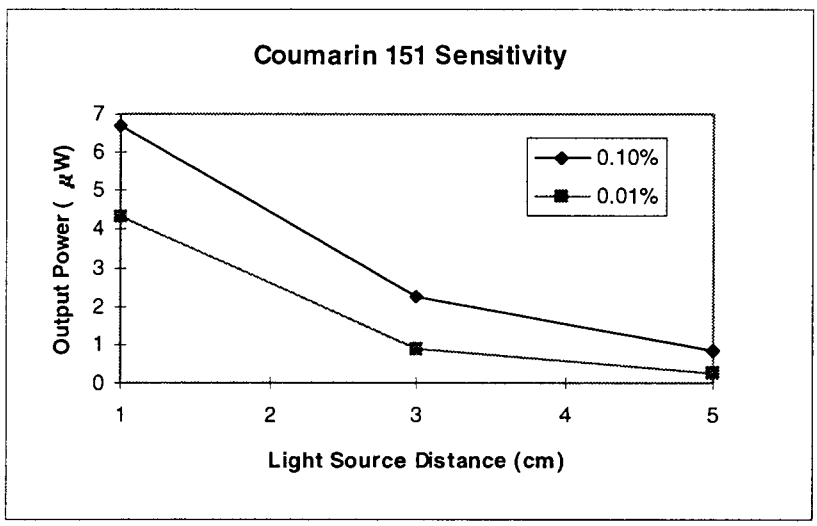

Figure 2.10 Coumarin 151 Grid Responses

Sulforhodamine 101 doped grids were fabricated later when the color processing capabilities became an issue. For those experiments, which are described later, it became apparent that the latter three dyes would not cover the visible spectrum sufficiently. So Sulforhodamine 101 grids were fabricated to provide better absorption near the red end of the spectrum. Other dyes were available which absorb at even longer

wavelengths, but they were found to be incompatible with the matrix material being used, or of such low quantum efficiencies as to be inadequate for this work.

Chapter 3

System Implementation

Now that the operation of photoluminescent concentrators has been explained, along with the rational behind using them for this project, it is time to examine the remaining components and function of the system. This chapter provides a complete description of how the macro scale LCs were incorporated into an electronic system and interfaced to a computer. Furthermore the processing functions which were realized in software, and their subsequent modifications, are examined.

3.1 Electronic Interface

There are three major stages to the electronics which made it possible to analyze the light signals collected by the LC grids:

1. **Optoelectronics** - to convert the optical signals into electronic signals.
2. **Analog Electronics** - for amplifying, sampling and multiplexing the analog electronic signals.
3. **Microprocessor** - to control sampling and multiplexing, perform analog to digital conversions, and transfer the digital information to a computer for analysis.

3.1.1 Optoelectronics

The primary function of this system as a whole was to detect incoming light signals, and the primary area detector chosen for this task was a photoluminescent concentrator patterned in the shape of a grid. To make use of the signals collected by the LC grid, it needed to be coupled to some type of optoelectronic device to transform them into electrical signals. Linear CCDs were eliminated as a choice due to their high cost, and the fact that have much higher resolution than was necessary for this large scale prototype. Prefabricated silicon photodiodes were chosen as an inexpensive alternative which would be simple to use, and still small enough to allow an adequate detector resolution sufficient for proof of concept.

Sharp BS100C photodiodes for visible light were used. The spectral characteristics are listed in Appendix A2.1. The creation of the macroscale LCs was somewhat limited to a 10 cm x 10 cm area due to the spin coating process of forming the thin film polymer matrix. The photodiode dimensions were such that when they were placed in a continuous line, sixteen of them would fit within 10 cm. This imposed the limit for the resolution of the line spacing to be used when patterning the LC grids.

The final issue which needed to be addressed was the manner in which the LC grid would be coupled to the photodiodes. In the integrated scale version, due to the planar nature of IC fabrication processes, the coupling would likely be as depicted below in Figure 3.1. However, for the macro scale implementation, due to the physical

dimensions of the photodiodes, an alternate method (Figure 3.2) of coupling the LCs was actually used.

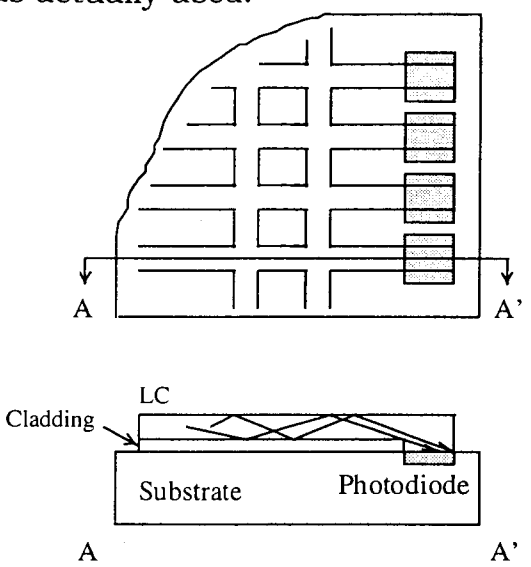

Figure 3.1 Coupling LCs to Photodiodes

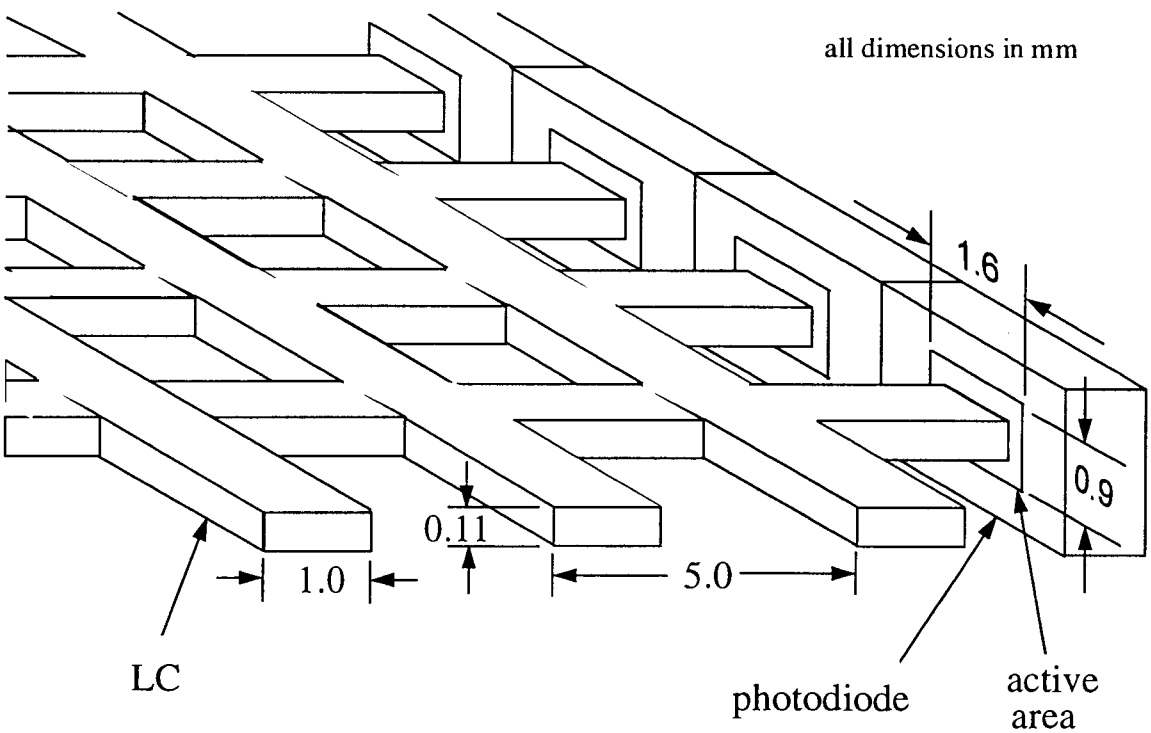

Figure 3.2 RFS Coupling Method

Ideally, in either of the above arrangements, there would be an antireflection coating between the photodiode and the LC to maximize the photon collection efficiency. For the microscale version, this would be relatively easy to implement, after fabricating the photodiodes, and prior to depositing the LC. With the macroscale version, it would not have been easy or very useful to apply an AR coating to the prefabricated photodiodes used.

With the butt coupling method employed, it was difficult to ensure that the end of every grid line was in direct contact with the surface of each photodiode at the same time. In many cases there was likely a small air gap between the two, which caused a reduction in efficiency which could not have been corrected with an antireflection coating. With the ends of the grid lines simply placed adjacent to the photodiodes there was a varying degree of coupling efficiency, due to random misalignment. To try to reduce this uncertainty, something close to the surface coupling method of 3.1 was used for the selective channel LCs used later.

One more important consideration involved in coupling the LCs to the photodiodes is that of shielding. In Chapter 2, graphs showing the sensitivity of the different types of LCs are shown. One thing to note is the intensity of the light measured coming out of the ends of the LC gridlines. At best it is on the order of microwatts. In order to keep the signal to noise ratio as high as possible then, the photodiodes must be shielded to ensure that only light from the LCs is detected, and not stray light from the source illuminating the LC.

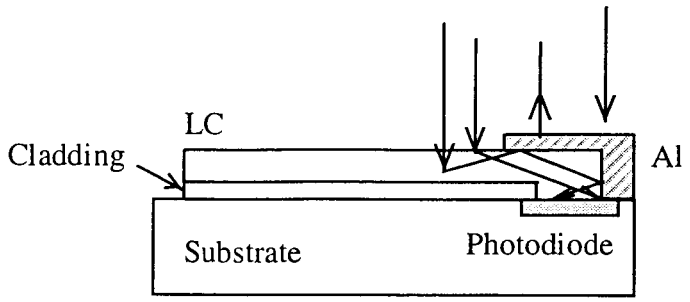

Figure 3.3 Shielded Photodiode

Shielding the photodiodes on the integrated scale version of the receptive field system could be accomplished simply by depositing a layer of aluminum as depicted in Figure 3.3. This can have a secondary function as shown - increasing the probability that light traveling to the end of the gridline does not simply escape out the end, but is reflected back toward the photodiode, thus improving the coupling efficiency. With the macroscale version, which used the butt coupling method for the grids, depositing a layer of aluminum to shield the photodiodes would have been problematic, so a different method needed to be employed. Black material was used to shield the photodiodes, but this may have contributed to further misalignment as mentioned previously. Furthermore, any light escaping the end of the gridlines, and not reaching the photodiode, would have been simply absorbed. So it did nothing to improve the coupling efficiency, but did improve the signal to noise ratio.

3.1.2 Analog Electronics

The following figure represents the analog electronic stage of the Receptive Field System, starting from the photodiodes and ending at the microcontroller stage.

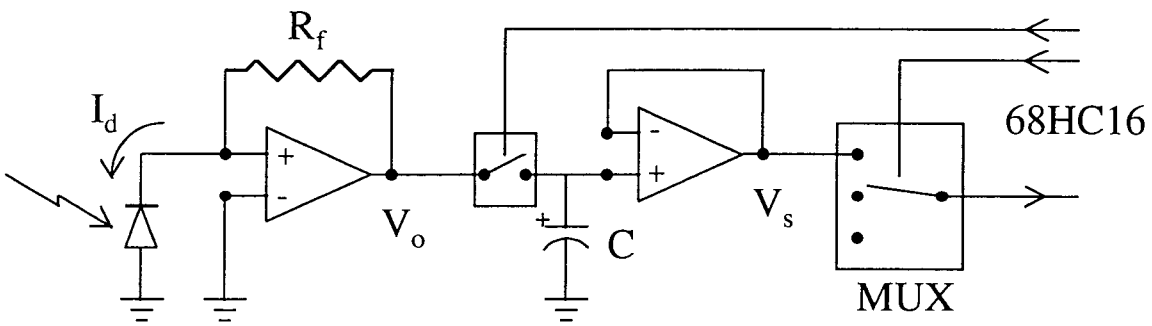

Figure 3.4 Analog Processing and Control Circuitry

Amplification

The light signals received by the LC were guided into the photodiodes which were operated in the photovoltaic mode. When used in this mode, they did not require a bias supply. Operating them in photoconductive mode would have required reverse biasing them, but would only have been necessary if fast response times were required (Horowitz and Hill 1989, page 996). When connected to the operational amplifier as shown, the result is a current to voltage converter which behaves according to the following equation (Horowitz and Hill 1989, page 1040):

$$V_o = R_f I_D \qquad (3.1)$$

It was experimentally determined that a resistor value of 5.1 MΩ would sufficiently amplify the photodiode current so that under the brightest lighting conditions used, V_o would not exceed 5 volts. This was to allow compatibility for the A/D converter at the microprocessor stage. Although in theory using a resistor greater than 1 MΩ in a feedback amplifier circuit could introduce unacceptable noise into the system, in practice the resistor value used did not cause significant problems.

Sample and Hold

The next section of the circuitry is a switch, capacitor, and unity gain buffer to provide a means for executing a sample and hold of the analog signals. While the switch is closed, the output V_s simply follows the analog voltage signal V_o and the capacitor is charged to the same level. When the signal from the microprocessor stage triggers the switch to open, the capacitor holds the voltage level V_o at that instant. The current draw from the high input impedance op amp is generally small enough so that the charge on the capacitor remains at that level until the switch is closed again. Until that happens, the output of the op amp V_s is held constant so that an A/D conversion can be performed at the microprocessor stage. The value of the capacitor is the most important parameter in determining the performance of the sample and hold. If it is large enough, it will hold its level for a reasonably long time in spite of the leakage at the switch and op amp. However, if it is too large, it will not be able to accurately follow a high frequency signal (Horowitz and Hill 1989, page 220). For this system, rapidly changing signals would only be caused by a light pattern moving very quickly across the surface of

the grid, or rapidly fluctuating in intensity. While motion tracking was to be tested, these extreme conditions were not, so a capacitor value of 0.1 μF was chosen.

Multiplexing

The last section before the microprocessor stage was the multiplexers. Since the on-board analog to digital converter only had eight channels, and there were 64 photodiodes (each with its own amplifier and sample and hold circuitry), some form of multiplexing was necessary. So eight 1 of 8 multiplexers were used to allow A/D conversions to be performed successively on all 64 signals. For consistency, all 64 signals were sampled simultaneously and held until the multiplexers could switch through all eight sets, allowing all 64 conversions to be performed.

3.1.3 Microprocessor

In order to mimic more of the functionality of the human visual system, the signals received by the optoelectronic hardware, and appropriately amplified and separated by the analog electronics, needed to undergo further processing. This could be accomplished by more sophisticated analog electronics (which will be discussed further), but eventually, to analyze its performance, it would need to be interfaced to a computer, so that the results could be displayed on screen. This is the justification for the last half of the analog electronics described in the previous section, and the microprocessor. It is needed to act as a low level controller for the sample and hold, and multiplexing stages, allows analog to digital

conversions to be easily performed, and provides a convenient interface to a desktop computer which could process the incoming information.

The microprocessor chosen for this task was the Motorola 68HC16 Microcontroller. Many other microprocessors and DSP chips are available which might have been chosen. However, this one was considered the most suitable for the task. Complicated signal processing routines, such as Fourier analyses, or filtering were not going to be used, so DSP chips which are superior to microcontrollers in this respect were ruled out. Other microcontrollers however, did not have the capability to perform on-board analog to digital conversions, thus necessitating a data acquisition stage which could perform this function to be installed before the controller. Some that did have A/D converters, either did not provide many channels (thus requiring more multiplexing), or did not perform the conversions with more than 8 bit accuracy. The 68HC16 had an on-board 8-channel A/D converter which could operate with up to 10 bit accuracy, and it could easily perform the minor control functions, and data transmission which was needed. The following flowchart outlines the functions the microprocessor performed. The complete assembly code is found in Appendix A3.

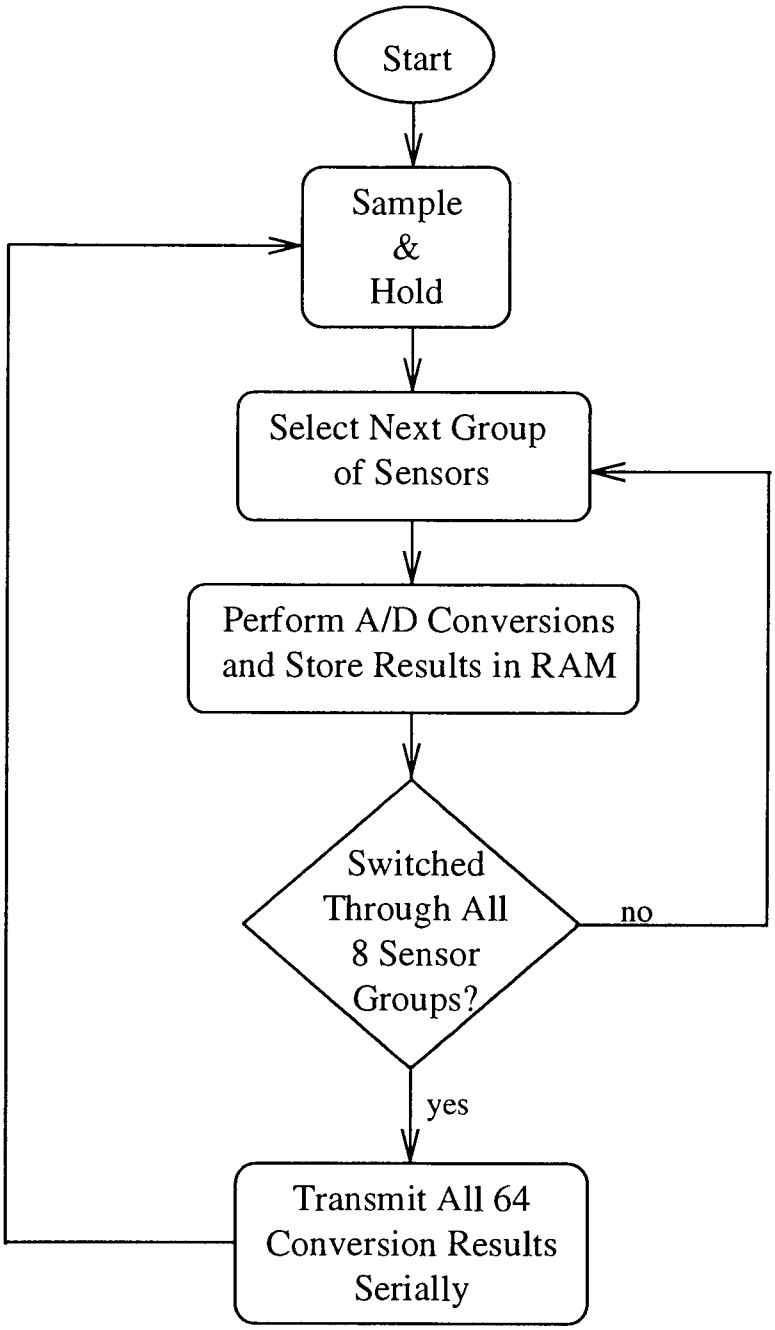

Figure 3.5 Microprocessor Control and Data Handling Flowchart

The first main function the microprocessor performs is signaling the switches in the analog electronics stage to open and close at the appropriate times. Initially, the switches must remain closed for a time,

to sample the incoming signals, and then open them to hold those values while the A/D conversions are performed. All the switches are closed simultaneously by setting the appropriate line high to which all the switches control inputs are connected. It was assumed that there would not be significant propagation delays between the stages, and essentially all the switches would actually close or open at the same time upon toggling that control line. Since the sampling rate was not very high, ensuring that all the switches actually open or close simultaneously was not very important. The main reason it would be required is if very quickly changing light signals were to be detected, which was not the case.

Once the switches were opened (i.e.: the signals were being held), it was necessary to perform the analog to digital conversions on all 64 signals. Each of the eight channels were connected to the output of a separate 1 of 8 multiplexer to which were connected the outputs of eight amplifier stages from eight different photodiodes. After A/D conversions were performed on all eight channels, the results were stored in a temporary RAM location, the multiplexers were signaled to switch to the next block of inputs, and the process was repeated. After this was repeated for all the sensor blocks, and all 64 results were stored in memory, the switches were closed for sampling the new incoming light signals. The conversions were performed with 10 bit accuracy with each conversion taking 10μs to execute. So this enabled all 64 conversions to be completed in less than a millisecond. So for the 0.1 μF capacitors chosen for the sample and hold circuits, the leakage current could be as high as 500 nA before a detectable difference between the first and last

signal conversion would occur. This is based on the following equation (Horowitz and Hill 1989, page 220)

$$dV/dt = I_L/C \tag{3.2}$$

and the fact that for a 10 bit conversion of a maximum 5 volt signal, an error in the last bit indicates a difference of less than 5 mV. According to the data sheets for the type of op amp and switch used, the leakage current would be approximately 100 nA.

The switches remain closed for the entire time the converted results are fetched from memory and transmitted serially to the p.c. via the RS-232 connection. The microprocessor was set to transmit the data at 9600 baud which was its maximum speed. Only after all the data was transferred was the process repeated from the beginning, and the signals were sampled again. Therefore, the transfer time had the most significant influence on the sampling rate. With 64 results to transfer, each 10 bits in length, the total transfer time would be about 65 ms, which is much larger than the time to execute the A/D conversions. So the sampling rate never exceeded 15 Hz which was adequate for tracking the motion of the light pattern incident on the grid. Of course this could be improved if necessary by using a faster microprocessor, or performing parallel rather than serial data transmission.

3.2 Software Processing

The processing of the light signals detected by the LC is useful and even necessary for determining how well the LC functions in the current

design. Also it allows determination, and duplication of preprocessing which is assumed to be done at the retinal level in the human visual system. The main functions to be tested are edge detection, size, shape, centroid and intensity gradient determination, motion detection, and color processing and extraction. Furthermore, software processing can help compensate for certain characteristics of the hardware, such as propagation losses in the LC.

3.2.1 LC Layout

Determination of the size, shape and edges of the incident light pattern can be done due to having detectors situated around the perimeter of the LC, but this by itself is not enough. The layout of the LC itself is quite important, and can make it easy, or nearly impossible to extract the size and boundaries. It definitely affects how the software processing functions need to be designed.

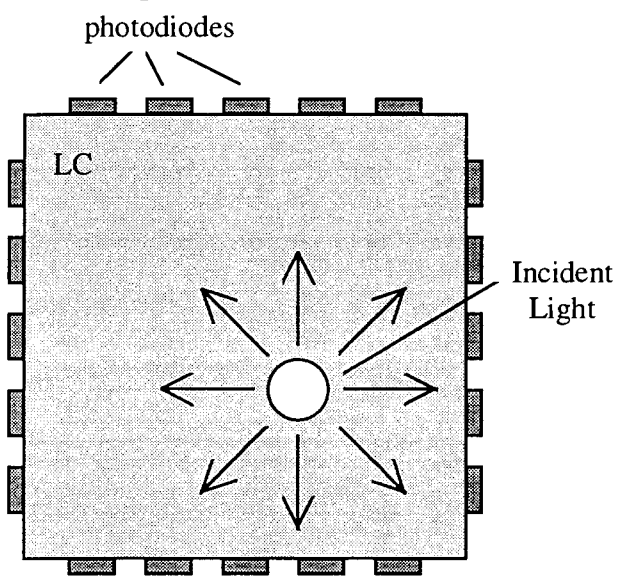

Figure 3.6 Simple Light Detection Scheme

With an arrangement as shown in Figure 3.6, light incident on the LC would produce some signal at all the photodiodes. Even the selective channel LC mentioned in the previous chapter would allow for signals at most of the photodiodes. These types of systems could not be easily used to determine the shape, size, or edges of the light pattern, without using more complicated processing algorithms and making large assumptions about the nature of the incident pattern. At best, it would be able to be used for determining the approximate position of the spot, since closer photodiodes would receive stronger signals based on the fact that there are propagation losses in the LC.

Experimentation with the selective channel LC (Figure 2.4 b) verified the above hypotheses. It was able to adequately locate the centroid of the incident light pattern and track its motion. However, it could not determine the boundaries of the spot. Furthermore, it had difficulties distinguishing between an increase in size versus an increase in intensity. It was essentially impossible to determine the shape of the object, other than roughly distinguishing between a linear shape and a more round shape.

By changing the layout of the LC to a grid (Figure 3.7), it is now possible to not only more accurately determine the position of the light pattern, but also its size, and describe a bounding box for its edges, which can give some indication about its general shape. If it is a circle, or square, the bounding box would be roughly square. If it is more of a linear pattern, the bounding box would be more rectangular, indicating the orientation of the incident pattern.

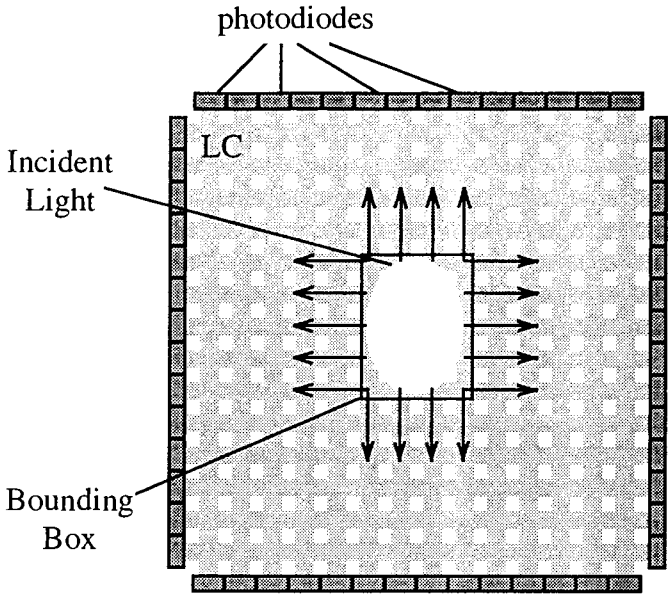

Figure 3.7 Grid Detection Scheme

3.2.2 Edge and Size Determination

Using the LC layout depicted in Figure 3.7 greatly simplifies the software functions to locate the edges of the incident light pattern which would then allow determination of its size and rough shape. Theoretically, light will only propagate down those lines which are illuminated which means that only the photodiodes which are connected to those grid lines will generate a signal. The rest will give no response (assuming perfect shielding from the light source, and other gridlines). Figure 3.8 shows actual intensity values received at two orthogonal sets of photodiodes when the grid is illuminated with a square light spot (assumed spatially uniform in intensity) covering the center of lines 7, 8, 9, and 10. With this kind of response (due to imperfect shielding, coupling, etc.), it is

necessary to set a threshold for properly interpreting the incident light pattern.

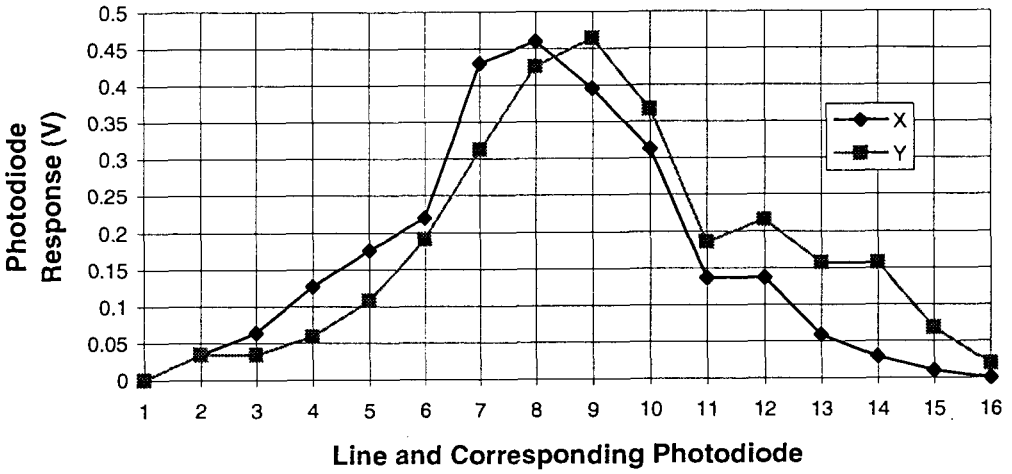

Figure 3.8 Photodiode Response vs Illumination Position

Based on the assumption that there is only a single contiguous spot of light incident on the grid, the software simply needs to check the data from the each of the photodiodes sequentially along two orthogonal sets of photodiodes (all 4 sets are not needed for a single grid). This allows determination of the bounding box as depicted in Figure 3.7. From this, the size, and orientation of the light spot with respect to the grid could be determined. The shape however, cannot be accurately determined. Consider the situation of Figure 3.9.

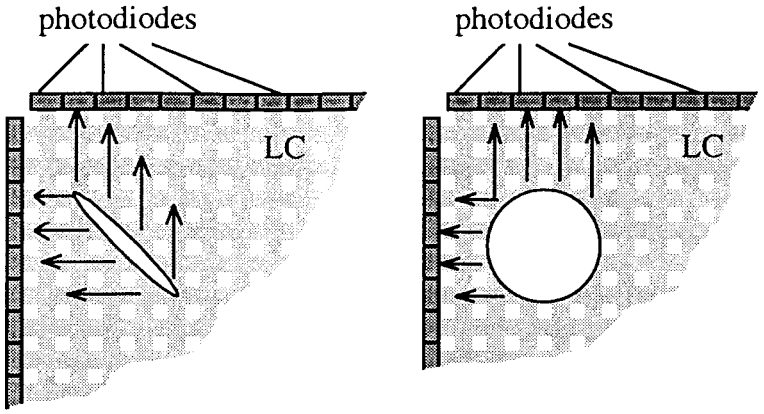

Figure 3.9 Shape Determination Problem

Both of the light patterns cause light to propagate along the same gridlines, activating the same photodiodes in each case. Therefore, the bounding box in both cases would be the same, a square containing the light pattern. This demonstrates how inadequate this method is at determining the shape, and in fact, even the orientation of the light pattern. The linear pattern could be rotated by 90 degrees, and it would still appear the same to the photodiodes. Only if the pattern were oriented along one of the grid line axes would orientation determination be possible. The only clue as to its shape and orientation could come from the relative strength of the signals at the photodiodes, but this assumes the incident light pattern has a spatially uniform power distribution, which it may not.

3.2.3 Centroid Calculation and Motion Tracking

Calculation of the centroid of the incident light pattern is also made easier, and more accurate by use of the grid shaped LC (Fig. 3.7) as

opposed to the simple square (Fig. 3.6). Furthermore, this does not rely on the assumption that the intensity of the light is spatially uniform. It requires only the input from 2 orthogonal sets of photodiodes, as before, one denoted as set X, and the other as set Y. The coordinates of the centroid (X_c , Y_c) can then be directly calculated from the following equations:

$$X_C = W \frac{\sum_{i=1}^{N} iX_i}{\sum_{i=1}^{N} X_i} \tag{3.3}$$

$$Y_C = W \frac{\sum_{i=1}^{N} iY_i}{\sum_{i=1}^{N} Y_i} \tag{3.4}$$

where X_i , Y_i are the signals from the ith photodiode in the X and Y array respectively, i is the number of the photodiode, N is the number of photodiodes in each array, and W is the distance between each gridline. From this, it is apparent that the smaller the spacing between each gridline, and the larger the number of gridlines, the better the accuracy of the centroid determination. For this system, W was 5 mm, and N was 16. An example of the centroid position for an arbitrary uniform light spot is depicted in Figure 3.10.

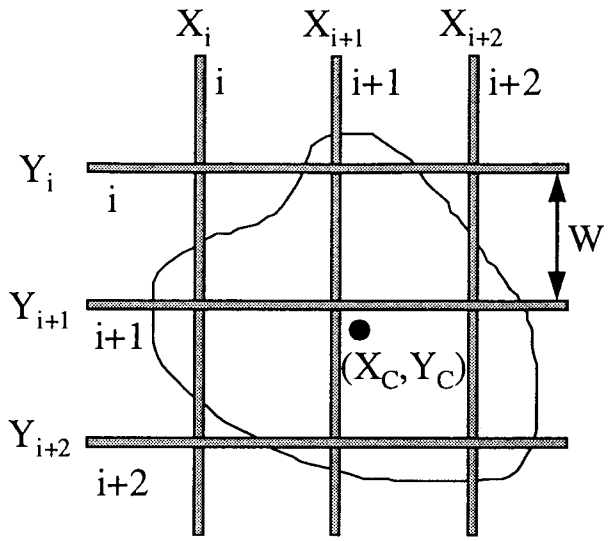

Figure 3.10 Centroid Calculation Example

One limitation of this is that the result only makes sense if the light pattern is a single spot. If there are more than one light spots of indeterminate shape incident on the LC, this calculation will give a position centered between them, and closest to the spot with the highest intensity.

The motion tracking capability of the system was realized simply by sampling the signals produced by the photodiodes in response to the incident light. If the position of the light pattern changed from one sampling period to the next, the intensity of the light at the photodiodes would change accordingly, thus affecting the signal input to the sample and hold circuitry. There is effectively no delay in the light pattern moving on the LC and the intensity changing at its edges since the response time for the photoluminescent material is on the order of nanoseconds (Schäfer 1977, page 29), and light propagation times through the gridlines would be even shorter. The photodiodes response

time is on the order of a few microseconds. So the limiting factor for tracking the motion is the sampling rate, which is about 15 Hz, as explained previously (Section 3.1.3). In this setup, the capability of the system to track the motion of the incident light pattern was simply tested qualitatively by observing the motion of the reproduced light pattern on the monitor. It would be a simple matter to calculate the time derivative of the collected light signals and from this extract the direction and speed of motion.

3.2.4 Shape and Intensity Gradient Analysis

At best, the previous calculations when combined would be able to produce on the monitor a rectangular box with a small spot inside representative of the boundaries and centroid of the incident light pattern. In addition, it would move across the screen in relation to the incident light's motion. However, this was still very far from reproducing the functionality of the human peripheral visual system. To this end, a more sophisticated algorithm was developed which made it possible to reproduce a much more detailed picture of the incident light pattern. It does this by calculating a specific illumination value for each crossing point or nexus on the LC grid which is illuminated. This nexus calculation determines which points are illuminated and which aren't by cross referencing each of the signals of an orthogonal set of sensors (e.g.: X,Y as denoted above). The following equation was derived experimentally based in part on the centroid calculations and initially as an attempt to provide software compensation for the propagation losses in the waveguides.

$$p_{mn} = \frac{x_m y_n}{\sum_{i=1}^{16} x_i} + \frac{x_m y_n}{\sum_{i=1}^{16} y_i} \tag{3.5}$$

The derived intensity at any intersection of gridlines is given by p_{mn} where m is the number of the gridline along the X axis, and n the number along the Y axis. The signals detected at the photodiodes connected to the gridlines which intersect are defined as x_m and y_n. Using this, each nexus which is illuminated can be accurately determined and represented on screen. In this way, a much better idea of the shape and orientation of the incident light pattern can be extracted from the received data. Also, it allows the identification of multiple light spots.

Figure 3.11 shows the results of performing the nexus calculation using the experimental data shown in Figure 3.8. Again, with the non-ideal response of the system (due to light leakage, poor coupling, etc.) it would be necessary to use thresholding in order to use the nexus calculation results to properly interpret the incident light pattern.

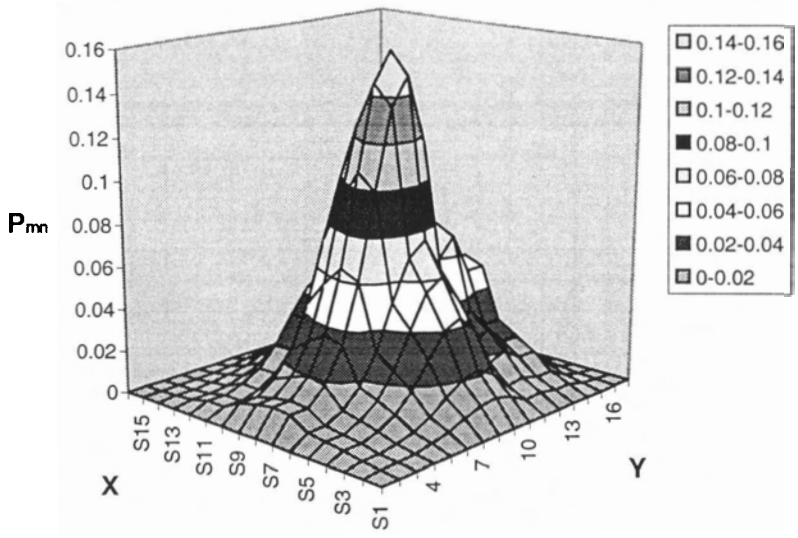

Figure 3.11 Experimental Nexus Calculation Results

In addition to giving shape information, the formula can allow a rough determination of intensity gradients since it gives a reasonable estimation as to the relative light intensity at each intersection point. The manner in which this was implemented is by drawing concentric ellipses around the centroid of the light pattern like a contour map. Each one indicates an illumination level drop of 20% the further away from the center it is. More sophisticated contour estimation and mapping could have been performed, but that was not the focus of this project.

In Figure 3.12, an illumination pattern as projected onto the LC grid is depicted on the left, and the corresponding pattern as reproduced based on the calculations mentioned above is shown on the right.

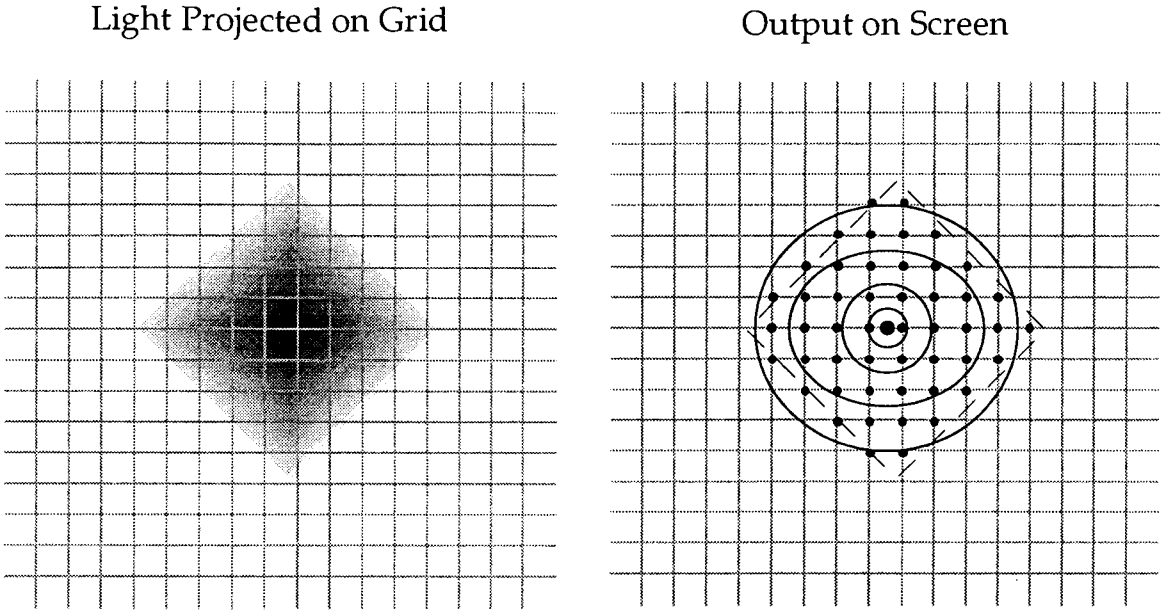

Figure 3.12 Nexus Calculation Example

The diamond pattern (or rotated square) on the right is shaded darkest in the middle to indicate the highest light intensity. On the left, everything except the dashed diamond outline would be displayed as shown after performing the nexus calculation. Every intersection point which is illuminated on the grid is marked with a circle, which allows the shape, size, and orientation of the light pattern to be determined. The larger circle in the very center which does not fall on an intersection point indicates the centroid of the figure. Finally, each of the concentric rings (some are slightly elliptical due to the location of the diamond pattern) represents the intensity variation which is highest in the center, and lowest around the perimeter.

The use of this formula yields a much better interpretation of the data which is collected by the system, and comes much closer to duplicating some of the functionality of the human peripheral visual system, but it does have some drawbacks. The algorithm is slightly more

complicated and must be performed N^2 times for an NxN line grid. This is not very significant for the macroscale version, but in the microscale which could have up to 100 lines per side it could become problematic. This could slow down the processing and its ability to perform useful motion tracking (assuming the data transfer process is not the limiting factor). Secondly, it does not necessarily allow recognition of much more complicated shapes such as printed characters, but would usually only be able to help the system distinguish between regular polygons.

3.2.5 Loss Compensation

With a slight modification, the equation 3.5 can be used to try to provide corrections in software for the propagation losses in the LCs. It still calculates an approximate light intensity for each intersection point on the grid, but by cross referencing the signals, it counteracts the propagation losses based on the distance through the grid the light traveled to reach the photodiodes.

$$p_{mn} = \frac{x_m y_n}{\sum_{i=1}^{16} \frac{x_i}{c_i}} + \frac{x_m y_n}{\sum_{i=1}^{16} \frac{y_i}{c_i}} \qquad 3.6$$

The equation is nearly identical, except for the inclusion of the loss factor c_i which was experimentally determined to be of the form

$$c_i = 10^{a(i-1)} \qquad 3.7$$

where the constant a is different for each type and concentration of dye used. For the grid doped with 0.01% Rhodamine 6G, a is approximately 0.2 which compensates for the losses of 3dB/cm. Since the losses are different for each type of LC, it would be necessary to recalibrate the system for each one to determine the proper loss factor to use. However before this could be done effectively, it would be necessary to resolve the problems with the losses due to coupling.

3.2.6 Color Extraction and Processing

Initially, it was assumed that all 4 sets of photodiodes would be needed to process the light pattern incident on an LC. The algorithms used for implementing the previous functions (size, shape, intensity gradient determination, etc.) only required the use of two orthogonal sets of photodiodes for a single LC grid. Once that was established, it became apparent that a second grid could be stacked on top of the first grid and coupled to the remaining sets of photodiodes (Figure 3.13), thus allowing the color processing facet of the artificial eye project to be explored.

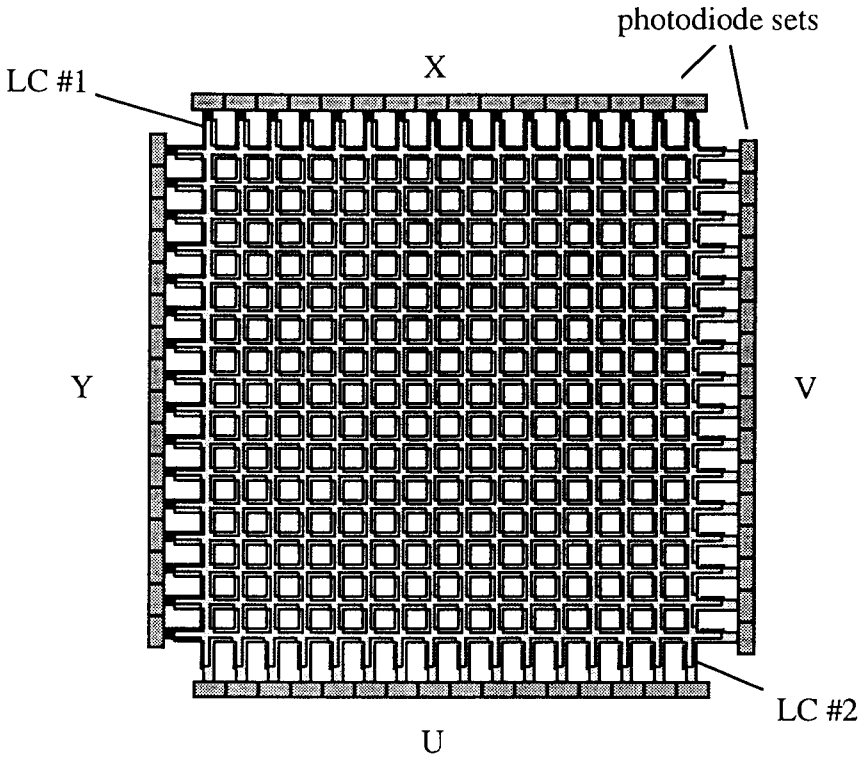

Figure 3.13 Two Grid Stack

After a second LC was connected to the system, minor modifications to the existing software allowed both grids to act independently. Each one was then capable of detecting the incident light pattern and the previous processing functions could be performed on both sets of data (now denoted X,Y and U,V). The real question to be answered was whether they could act interdependently, taking advantage of the different spectral absorptions of each LC, each having been doped with a different dye, to separate out the spectral components of the incident light.

Initially, the system was tested to see how the two stacked grids would each respond to two different light spots approximately matched to the absorption characteristics of each LC. The top grid had been doped

with Sulforhodamine 101 with a peak absorption of 578 nm, and the bottom grid had Rhodamine 6G with a peak absorption of 530 nm. One spot of light projected onto one section of the grids was created using white light which passed through a red broadband filter, and the other spot was generated with white light passed through a green broadband filter. As expected, the top grid had a stronger response to the red light spot and tracked it, while the lower grid tracked the green light spot. However, each grid did not respond exclusively to the specific light spot which was matched to it. The position of the centroid calculated for each grid did indicate that the top grid was also picking up some of the signal from the green light spot, and the opposite was true of the bottom grid.

Several explanations could account for the non ideal performance of the system. While each grid does respond maximally to a specific wavelength, their actual absorption bandwidths are about 50 nm. Also, the light spots were not spectrally pure, or perfectly matched to the absorption peaks of the grids - they were white light (of indeterminate spectral content) filtered through broadband gel filters. These factors alone could explain the responses of the grids to both light spots. Other reasons might be cross talk between the grids. The two grids were not separated by a cladding layer since a suitable material (thin, transparent and with a refractive index < 1.5) was not readily available. So the light propagating through the grids may not have been trapped by TIR at the interface between them. Furthermore, the emission peak of Rhodamine 6G (556 nm) is close to the absorption peak of the Sulforhodamine 101 grid. After light was absorbed by the bottom grid, and shifted up to the emission band, any of that light which escaped, would likely have been absorbed by the top grid.

The next test to be performed used a single white light spot projected on the grids. The software was modified to force the signals collected by the grids to be combined for output on the screen in the same proportions as the incident light pattern. The light collected by the Sulforhodamine 101 grid would contribute to the amount of red in the output on screen, and the Rhodamine 6G grid output would contribute to the green output on the screen. In this manner, it was hoped that not only the centroid, size, and shape of the incident light pattern could be reproduced, but the color as well. Not every possible color would be able to be reproduced, since that would require three grids for full RGB detection, but it should work adequately for any mixture of green and red.

When the grids were illuminated with a white light spot, the output on the screen was yellow which was to be expected. It indicated that near equal amounts of green and red were present in the light and detected by the grids. When green and red light is mixed in equal quantities, the result is yellow. With a third grid sensitive to blue in the system, it would have detected and contributed a certain proportion of blue light to the output on the screen resulting in a white light spot.

One problem noticed however, relates back to the coupling problems, and propagation losses. The colour reproduced on the screen would change if the position of the of the incident light spot was moved away from the center of the grid. Furthermore, the brightness of the spot on the monitor was much lower than the incident spot. This problem was artificially corrected simply by scaling up the signals in software. But the obvious reason for these problems is that the grids were not sensitive enough and had too many losses. These problems would not

necessarily be as severe in a microscale version with much better coupling and smaller distances for the light to travel and hence fewer propagation losses. However, it would have made performing more quantitative tests difficult, and likely yielded inconclusive results. To counteract these losses, the selective channel design for the LCs was used for performing the quantitative testing of spectral responses and color processing detailed in the next chapter.

Chapter 4

System Testing

The feasibility of developing this system to perform color processing in addition to shape, size, intensity, and motion information was based on known and theoretical responses of the individual components. While the previous chapter indicated how the hardware and software were integrated to provide for some of the desired functions, this chapter describes the experiments and results obtained from testing the response of the system as a complete unit. Specifically, the spectral sensitivities and absolute thresholds of the system are measured using LCs doped with the dyes mentioned previously. In this way, the concept of using multiple stacked LCs in order to realize color processing is proven. The details of how the experiments were carried out are included in Appendix A5. For these tests, the LCs used were not the grids, but rather in the selective channel layout depicted in Figure 2.4 (b).

4.1 Area Summation Effect

The sensitivity of the system to incident light patterns of different areas was tested and the results are shown in Figure 4.1. The system responds in a linear fashion proportional to the area of the LC stimulated. The interpolated line was determined using the least squares fitting method and indicates that the slope is nearly unity.

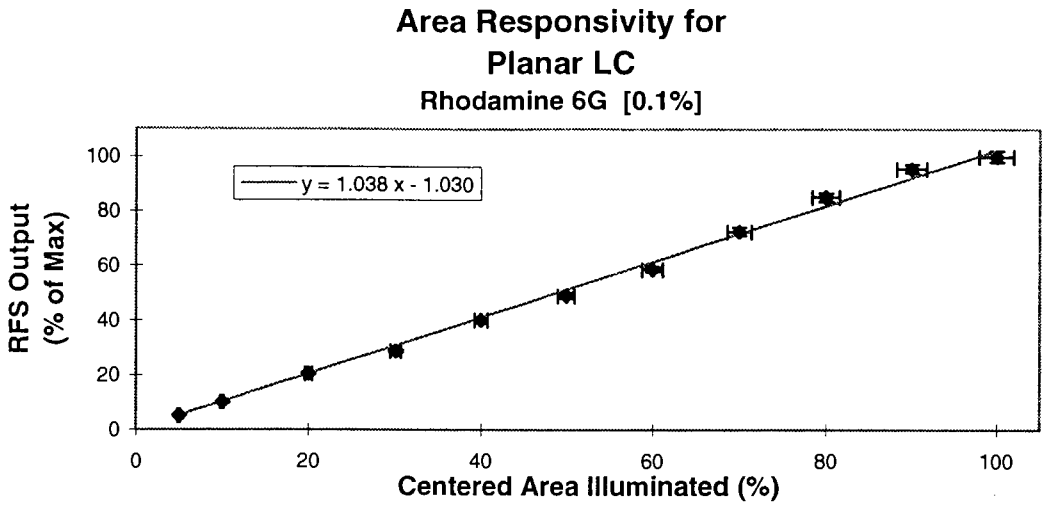

Figure 4.1 LC Area Sensitivity

4.2 Spectral Sensitivity

The sensitivity of the system to light of known spectral content was measured with a variety of LCs and LC layering configurations. The following graphs have similarities to the spectral absorption characteristics of the particular dyes used in the LCs. However, the photodiode spectral sensitivity also contribute to the responses, and for measurements made with more than one LC, it is evident that there were interactions between them. The photoluminescent dyes used for the LCs of these experiments were Sulforhodamine 101, Rhodamine 6G, and Coumarin 6, in order to cover the long, medium and short wavelength regions of the spectrum.

4.2.1 System Responses Using Individual LCs

The first parameter to be considered is the spectral response of the RFS which is determined by the particular LC used. The curves were obtained by passing white light through a series of narrowband filters and adjusting the incident light power to a constant level of 20 mW. The photodiodes receiving the signals from the LCs would respond to light of any wavelength within their spectral sensitivity range. Although the LCs would absorb light at one wavelength and re-emit at a longer wavelength, there was no way of measuring what this wavelength was using the RFS. It was assumed that for a particular photoluminescent material, for the range of wavelengths which would be strongly absorbed there would be a correspondingly strong emission spectra (Stoke's shifted), which would be detected by the photodiodes. Figure 4.2 shows the RFS responses when each of the three dyed LCs were used as the sole LC in the system.

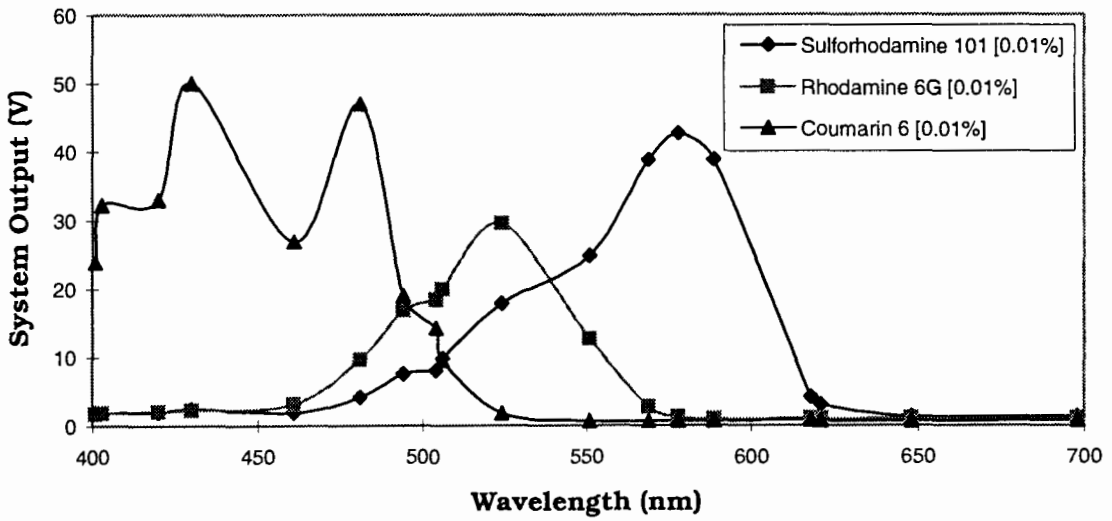

Figure 4.2 Spectral Sensitivity of RFS for 3 Dyes

The shapes of the spectral sensitivity curves for the LCs doped with Sulforhodamine 101 and Rhodamine 6G closely match the spectral absorption curves for those dyes measured in ethanol. However, the same is not true for the curve for Coumarin 6. The absorption curve for Coumarin 6 does indicate strong absorption from 400 - 500 nm, but it only peaks once at 458 nm. This suggests that while Coumarin 6 does absorb at 458 nm, absorption of this wavelength does not result in a strong emissive response, but likely triggers a non-radiative energy transition. This could be due to age related decomposition of the photoluminescent material.

The LCs used for the above measurements were all doped with the same concentration of the particular dyes used (0.01%). However the dye concentration was not found to affect the shape of the spectral sensitivity curve. Also, using a higher incident power level does not significantly affect the shape of the curve either. Only the level of response is affected when either of these parameters are changed. The following graphs demonstrate the uniformity of shape for the curves when those parameters are changed.

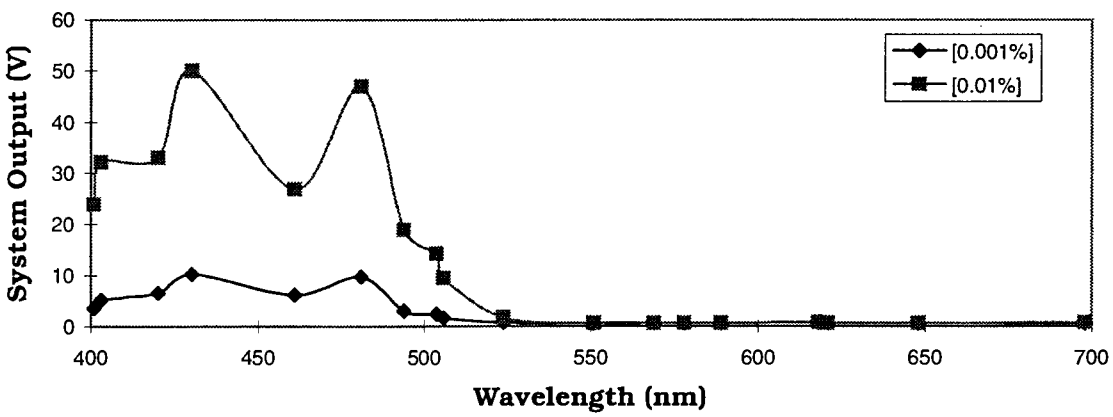

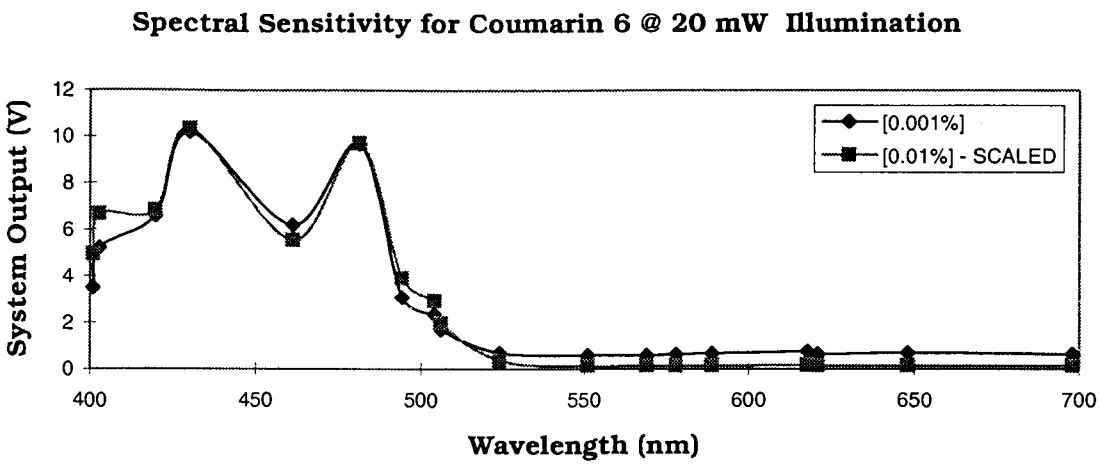

Figure 4.3 Effect of Dye Concentration on Spectral Response

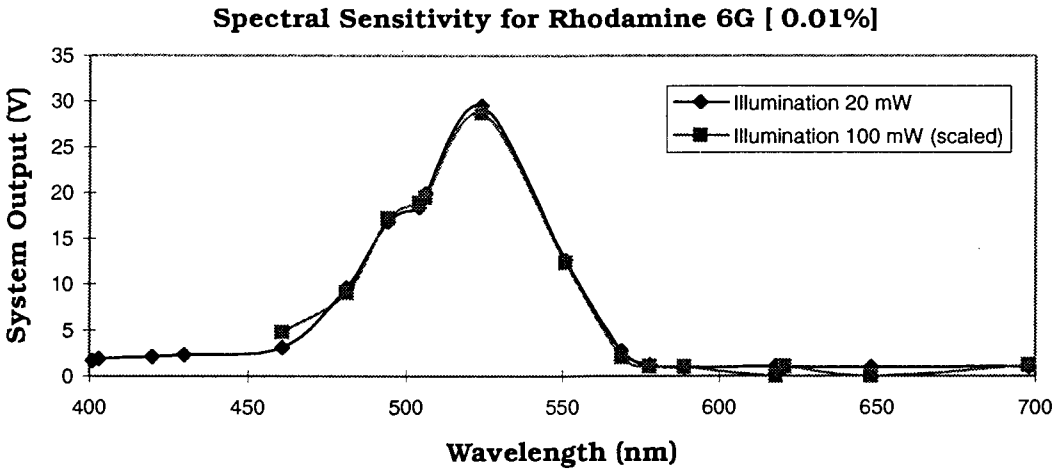

Figure 4.4 Effect of Illumination Level on Spectral Response

One other thing to note about Figure 4.3 is that the response for [0.01%] Coumarin 6 needed to be scaled down. However this does not follow from the graph of Coumarin 6 loss vs concentration in Chapter 2 (Figure 2.5) which indicates that the lower concentration should give a stronger response. The only difference is that the measurements for Figure 4.3 were made on the selective channel LCs, rather than LCs patterned in the shape of grids. This could suggest that for a fixed dye

concentration, not only the thickness of the LC but also its planar geometry can affect the responsivity.

Figure 4.4 shows two spectral response curves for the RFS using an LC with Rhodamine 6G [0.01%] which overlap very closely. However, the curve for the response for an illumination level of 100 mW does not extend all the way to 400 nm. The reason for this is that the light source used was close to CIE Illuminant A which does not have as much power in the blue region of the spectrum. So using the interference filters to block all but the blue light resulted in reducing the illumination level below 100 mW, even with the lamp voltage at maximum. In spite of this, it is clear that the LCs respond nearly identically over a range of incident power levels.

The next thing which needs to be considered then, is the absolute sensitivity of the RFS system to determine its dynamic range as a function of the LC used.

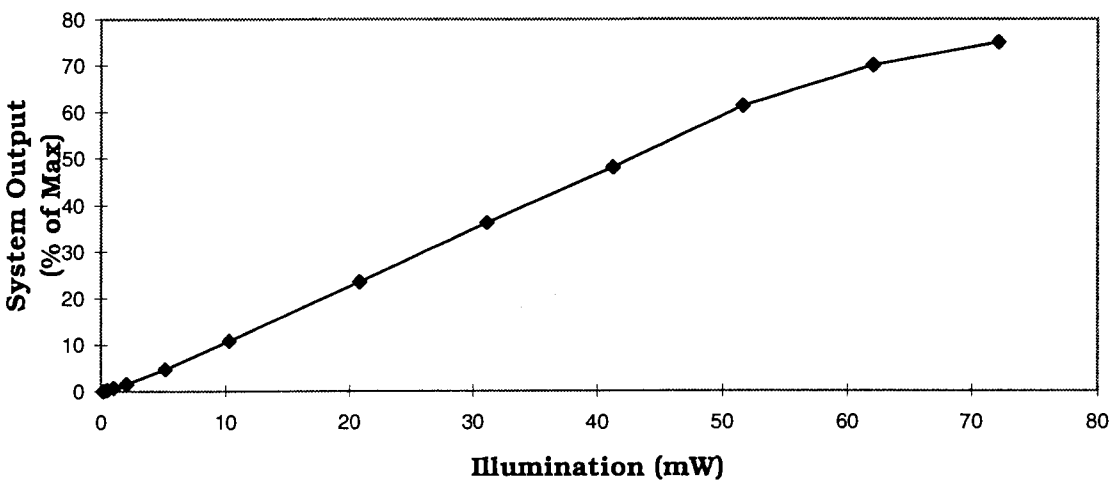

Figure 4.5 System Sensitivity @ 481 nm for Coumarin 6 [0.01%]

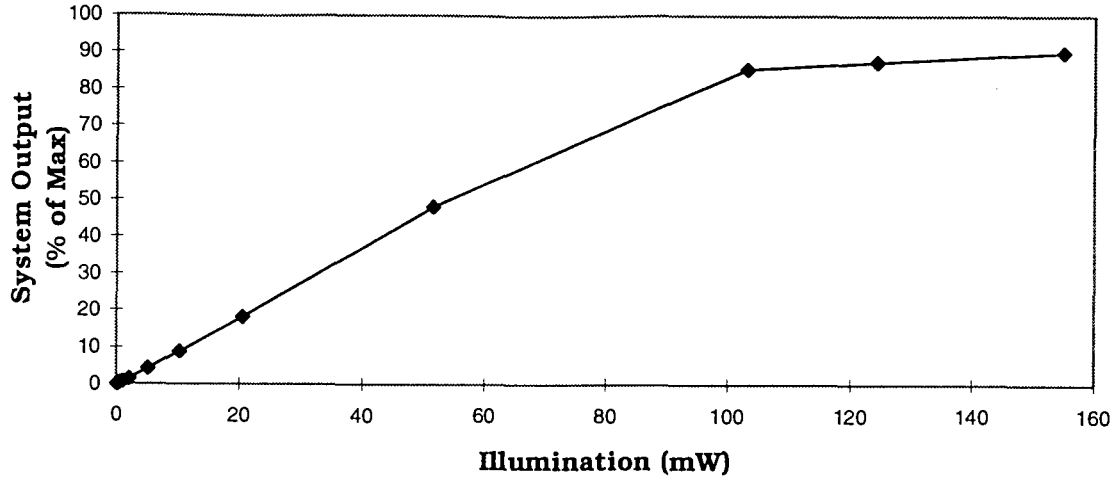

Figure 4.6 System Sensitivity @ 524 nm for Rhodamine 6G [0.01%]

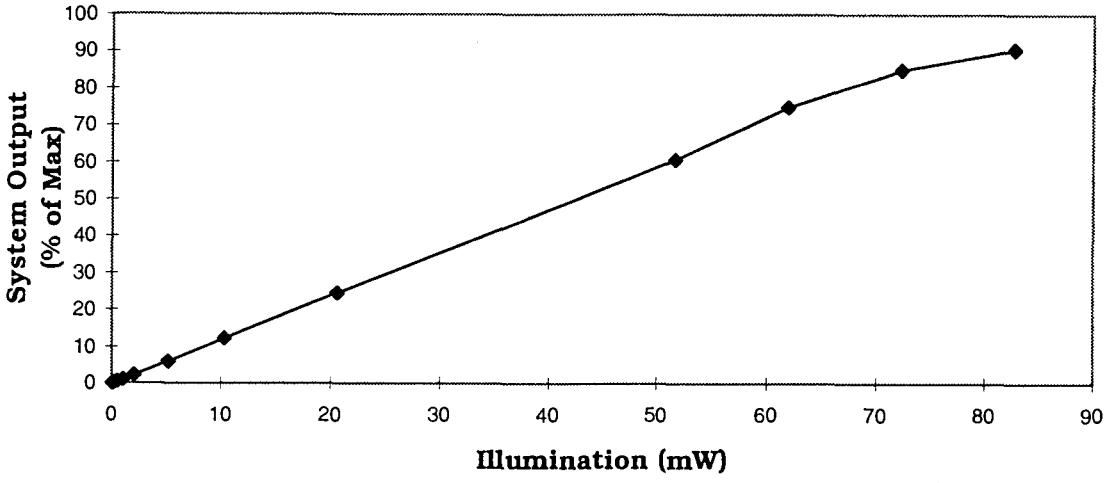

Figure 4.7 System Sensitivity @ 578 nm for Sulforhodamine 101 [0.01%]

The graphs in Figures 4.5, 4.6, and 4.7 show the functional sensitivity of the RFS for when an LC with a particular dye is used. For each one, the responses were tested at the wavelength which corresponded to the absorption peak of the dye in that LC. It was assumed that since these wavelengths gave the strongest responses for

one power level, it would remain true regardless of how much power was used. In each graph, the response of the RFS increases in a linear fashion for no illumination until it approaches the upper threshold where it seems to begin to plateau.

The response is indicated as a percentage of the maximum output (i.e.: all the photodiodes connected to the LC were saturated) which occurred for bright full spectrum light. However, as is apparent from the graphs, it was not possible to reach the maximum in any of the three cases illuminating the LCs with the filtered light. The reason for this may be the fact that the filters drastically cut most of the available illumination power from the light source (even at full power), as explained previously. It does not seem likely that it was caused by saturating the photodiodes, or exceeding the LC's light collection capacity since higher responses were possible with unfiltered light. However, it is reasonable to assume that if bright enough monochromatic light were used to illuminate the LCs, the response would eventually plateau for these reasons.

Something to note is that regardless of the LC used, 20 mW illumination is roughly in the center of the linear region of the response curves. This is important because the spectral sensitivity measurements were performed using 20 mW illumination for the filtered light. If the curves of 4.5, 4.6, and 4.7 do level off at higher levels of illumination because of some inherent property of the LCs or photodiodes, then measuring the spectral responses at higher illumination might have adversely affected those measurements.

The last thing to discuss is the different ranges of power used for measuring the responses for each LC. This can be attributed to the same

problem as before. Since the light was filtered, the maximum level of illumination depended on how much power at a particular wavelength the light source could provide, and the optical density of the particular filters. Unfortunately, this prevented conclusive determination of the upper illumination limit which the RFS could handle.

4.2.2 System Responses Using Stacked LCs

Once the responses of the system were tested using individual LCs, it was retested at 20 mW illumination with the different possible configurations of stacked LCs. The RFS was only capable of handling 2 LCs at once, so all three LCs with Coumarin 6, Rhodamine 6G, and Sulforhodamine 101 could not be tested simultaneously, so they were tested in pairs. In the following graphs, the legend indicates the second LC stacked with the primary one, and whether it was above or below.

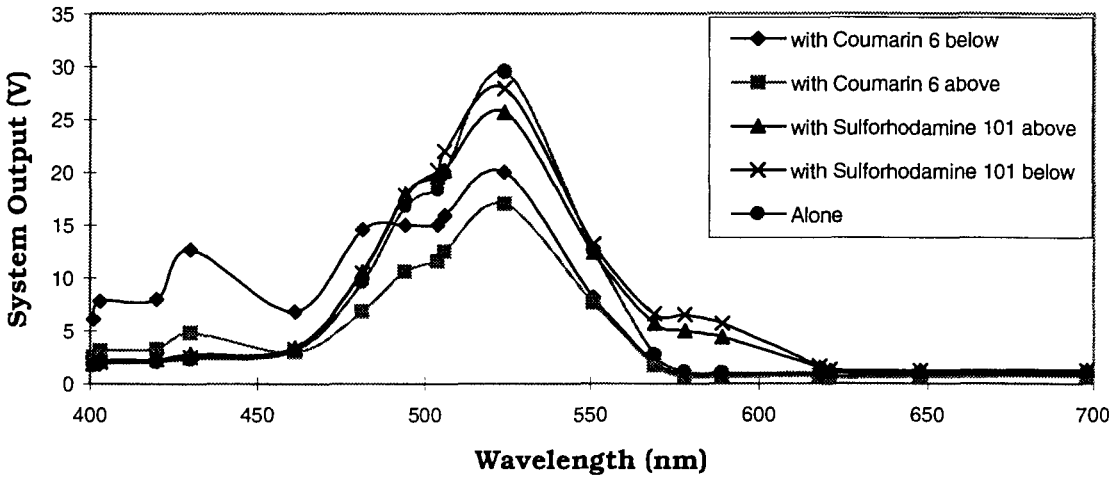

Figure 4.8 Variations on Spectral Sensitivity for Rhodamine 6G

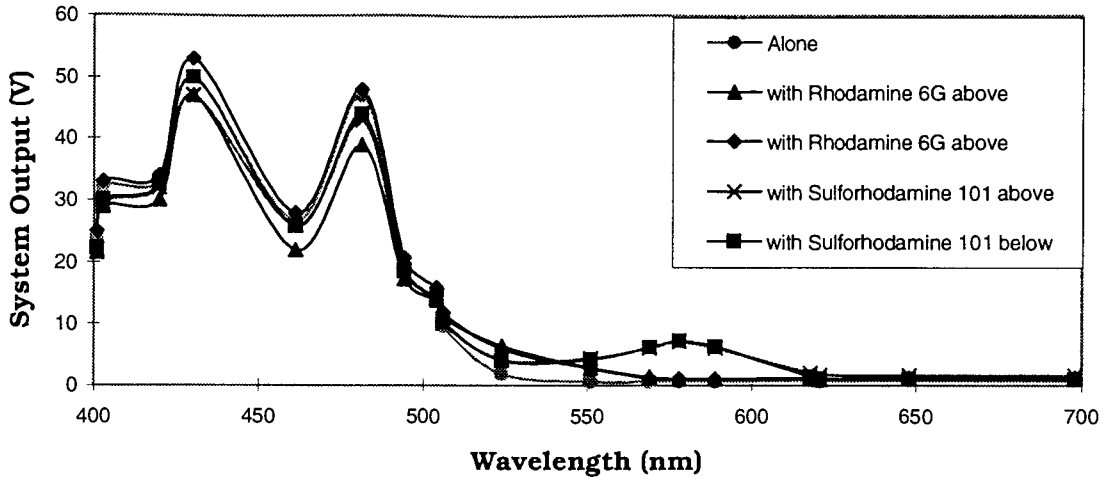

Figure 4.9 Variations on Spectral Sensitivity for Coumarin 6

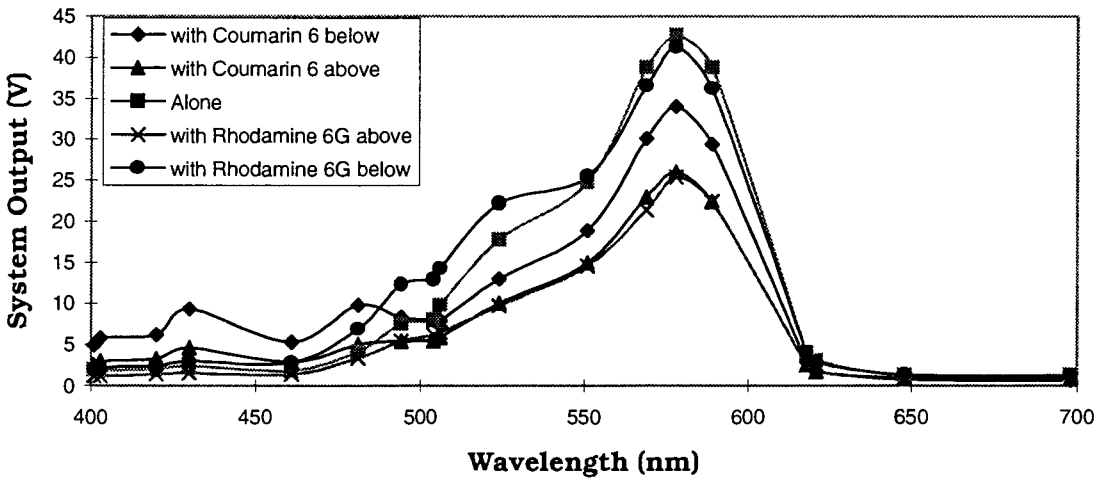

Figure 4.10 Variations on Spectral Sensitivity for Sulforhodamine 101

For the most part, the effect on the spectral sensitivity of the RFS when two different LCs are stacked is not very significant. The absorption peaks remain essentially the same with some slight increase or decrease in response. As well the absorption bandwidth is not significantly changed. There are however a few striking exceptions.

When an LC doped with Coumarin 6 is stacked with an LC doped with Rhodamine 6G, there is a strong interaction between them. The Rhodamine 6G response demonstrates a second peak at 430 nm corresponding to one of the main peaks of Coumarin 6. This peak is much more noticeable when the Coumarin 6 LC is underneath the Rhodamine 6G LC. Similarly, the strong response at 578 nm for the Sulforhodamine 101 LC is seen in the other LC response curves when they are stacked with that LC.

The likely reason for its occurrence is that the light absorbed and then reemitted by the photoluminescent centers in the LCs is not effectively trapped within the particular LCs by TIR. So a percentage of the light emitted by one LC is transferred to the adjacent LC. This leakage would occur at the interface between the two LCs, and might be corrected by placing a transparent layer of lower refractive index between them. This also partially explains the corresponding overall decrease of the responses compared to the responses for the LCs measured alone. The other reason for the decrease in response is that the top layer would obviously absorb a certain percentage of the incident light, resulting in the bottom layer to be exposed to a lower amount of power.

Through the course of these experiments, it was possible to estimate the percentage of light absorbed per layer on the order of about 10%. However, each layer only absorbs preferentially the wavelengths corresponding to the absorption spectra of the photoluminescent material used. Furthermore, the use of an aluminum back reflector likely increased the amount of light injected into each LC.

4.3 System Error Analysis

While there were many sources of error in the system, the exact errors were never quantitatively determined since this was only intended as a test bed for different components, configurations, and LCs to help in designing a future microscale version. The errors in this system would not necessarily be directly correlated to errors in the future system, fabricated on an integrated scale rather than with discrete components. The errors which were present in this system however, were not usually of a magnitude to significantly interfere with the testing of different spatial processing functions, or different LCs and stacking configurations. Based on the data collected for the spectral sensitivity and dynamic range measurements, the total system SNR is roughly 50:1.

Although they were not precisely quantified and may not be directly correlated to future prototypes, the relative effect of different parameters was clear through experimentation. The significant ones are listed below in decreasing order of impact.

Light Leakage

The amplification circuitry for the photodiode output was built based on the assumption that the photodiodes would only be exposed to the relatively weak light signals from the LCs. As a result of the necessarily high sensitivity, any light from the illuminating source reaching the photodiodes directly or indirectly caused the RFS system to misjudge the actual shape, size, intensity and position of the incident light spot. This lead to a number of attempts at shielding them from all light but that

coming from the LC before the RFS could accurately recognize and track the incident light pattern. However, the method of shielding also depends on the type of coupling between the LC and the photodiodes.

Coupling and Propagation Losses

As previously mentioned, butt coupling of the LC to the photodiodes, would likely provide a higher level of light to be incident on the active area of the photodiodes than surface coupling. However it also allowed for a greater possibility of misalignment of the free-standing LC structures which causes a high degree of variability in signals detected at each photodiode for uniform illumination of the LC. So for more uniformity, and easier alignment, surface coupling was used, which likely wasn't as effective as it could be due to the limited area of contact between the LC and the photodiodes' active areas.

Propagation losses of the fluorescent light in a photoluminescent concentrator layer can arise for many reasons, and this has been touched on previously. The most common reasons are the critical cone losses which can be enhanced by the LC pattern, scattering centers in the matrix, irregularities at the surfaces making efficient TIR trapping difficult, and self-absorption of the light by the photoluminescent material (leading to concentration quenching in the extreme case) or the matrix material itself.

Electronics

The electronics used to convert the light signals collected by the LC into electrical signals to be passed to a computer for analysis likely introduced some amount of error. Up to the A/D conversions in the microprocessor, there are many sources of noise which could affect the final signal levels. These include fluctuations of the incident light, detector noise such as Johnson noise, generation-recombination noise, and frequency dependent noise, and RF interference picked up by the amplification circuitry (Dennis 1986, page14). The A/D converter had 10 bit accuracy, resulting in a minimum error of 0.098 % or 5 mV. Finally, all of the electrical components would be subject to power fluctuations and thermal drift but these would likely be negligible.

Chapter 5

Conclusions

The following conclusions and suggestions for future work are written in light of the overall goal of this work and intended contribution, that being the advancement of building a sensor capable of acting as an artificial eye for humans. The receptive field system was a large scale prototype built as a test bed to aid in the design of an integrated scale receptive field chip to perform detection and early processing as is done in the periphery of the human retina.

5.1 Results and Contributions

This work grew out of previous research of luminescent concentrator technology and proposed applications for the technology. Several characteristics of Photoluminescent Concentrators made them an attractive choice for the artificial eye project. Among these are the simplicity, passive (i.e.: powerless) operation, and flexible configurations. This flexibility applies to: the range of photoluminescent materials available offering a broad possibility of spectral sensitivities; the fact that they can be patterned in any planar shape and deposited on a multitude of surfaces; their ability to be stacked allowing for three dimensional (rather than merely planar) devices.

The previous research established a UV curable matrix material for the LCs making patterning a simple task, and demonstrated their ability to be incorporated into an integrated optoelectronic device. This thesis

demonstrated advanced use and incorporation of LCs in an optoelectronic system and highlighted some of the technical difficulties associated with realizing such a system.

5.1.1 Stacked LC Configurations

It has been shown that color extraction and processing of light signals can be accomplished by stacking appropriately doped LC layers and connecting them to independent sets of photodetectors. Although for this work, the three types of LCs tested had spectral responses which overlapped and covered the visible spectrum, this would not be necessary in all cases. But this allowed demonstration of the fact that broad spectrum light can be analyzed using such a system since each LC would respond maximally according to its particular spectral absorption characteristics. In this way, the color of the light and relative intensity of different wavelengths can be extracted since the LC characteristics would be known. However, the order of layering LCs affects the spectral responses to some degree due to absorption. So it would be important to establish what interactions occur between different LCs and whether or not these can be minimized in some manner.

5.1.2 Dynamic Range

The RFS was able to detect light levels across at least three orders of magnitude ranging from 100μW to 100 mW. It is likely that this range was limited by the sensitivity of the photodiode detection circuitry to

which the LCs were coupled. Ultimately, the dynamic range of any system incorporating LCs would likely be limited by the response characteristics of the optoelectronic transducers to which they were coupled. In this case, the photodiodes which were operated in photovoltaic mode would have only had a dynamic range of about 2000 (Chamberlain and Lee, 1984).

The illumination levels to which the RFS responded were also measured using photometric techniques in order to compare it to the sensitivity of the human retina. The system responded to illumination of 1 lux to > 1000 lux for the Coumarin 6 LC, and responded in a similar fashion for the others. These absolute brightness sensitivity measurements indicate that LCs can be used to develop a sensor with a dynamic range approaching that of the human retina operating in the photopic range. Photopic vision is defined by operation of the eye when adapted to high levels of illumination in which the cones are capable of detecting light, and occurs for levels greater than 10 lux (Le Grand 1968, pages 113, 123).

5.1.3 Information Extraction

By experimenting with the RFS while using the selective channel LC design, it was shown that it is not necessary to use very sophisticated LC layouts (e.g., grids) for performing information extraction and processing similar to that done in the periphery of the human visual system. Rather, simpler LCs can be used allowing higher efficiencies in capturing incident light, while retaining the most significant information, size/intensity, centroid, motion tracking, and color. This is useful for the

artificial eye project since it keeps the computational complexity involved in the information extraction low. That is important because the end goal is to eliminate the need for external processing by converting the functions currently performed in software to analog electronic circuitry performing equivalent operations on the signals directly.

By using the grids, it was shown that it is possible to use these and more sophisticated software algorithms to extract much more information about the incident light patterns. Although this may not be necessary for the artificial eye, other applications could definitely benefit from better information processing. It has been demonstrated that in addition to the above, boundaries, size, shape, orientation, and intensity gradients of images can be determined. With further improvements in resolution and reduction of losses, and even better software processing, all the image processing currently performed on data collected with CCDs could likely be carried over to LC based systems.

5.2 Improvements and Future Work

5.2.1 Photoluminescent Materials

Finding dyes with spectral sensitivities closer to those of the long, medium and short wavelength cones in the human retina could be pursued. Even though the spectral response curves for the RFS system using the LCs with the three different dyes do not match the spectral response curves for the cones of the human retina, the characteristics necessary for color processing are present. The curves all cover a broad portion of the visible spectrum, and there is significant overlap between

them. Ideally, the blue response would only have a single peak and the red response would extend up to 700 nm. However, with further testing, other photoluminescent materials can likely be found which can satisfy these conditions.

Further experimentation with determining appropriate concentrations of the photoluminescent materials to maximize the system responses would need to be done. This would need to be done separately for the macroscale version and microscale version due to the different LC dimensions (primarily thickness). Also, determination of the correct stacking order of the LCs for optimal signal strength at each layer would need to be done. Finally, experimentation with mixing dyes in one LC was not investigated, but might allow for superior spectral responses, closer to that of the cones in the human retina.

5.2.2 LC Geometry

More experimentation with exact LC geometry (both with selective channel acceptance angles, and gridline spacing, dimensions, width/thickness ratio, etc.) might be indicated to achieve lower losses, higher conversion efficiencies, etc. However, small scale versions would likely require different parameters than the macroscale system since thickness, area, and detector spacing would be drastically reduced. Also, the microscale version would likely use a parallel coupling method for transmitting the signals from the LCs to the photodiodes. The exact dimensions of photodiodes and distance the LC overlaps them would need to be determined to optimize the signal coupling.

5.2.3 System Enhancements

One necessary addition to the macroscale system, and any subsequent scaled down versions would be an imaging lens to focus the incident light patterns onto the plane of the LC(s). This would increase the sensitivity by magnifying the incident power of the incoming light signals. Additionally, apertures or neutral density filters could be employed to extend the upper threshold before saturation of the LC or photodiodes occurred. In these ways, the overall dynamic range and performance of the system could be improved.

5.3 Parallel Work

The integrated scale version of this system has in fact been developed in parallel to the macroscale receptive field system. However, many parameters could not be finalized until testing with the macroscale RFS were completed. However the basic initial concept of the integrated scale version is depicted in Figure 5.1. The photodiodes and processing electronics would be created on a silicon wafer using standard microelectronic fabrication techniques. Once that was done the LC layer could be deposited and patterned directly overtop of the photodiodes, and any subsequent shielding layers or antireflection coatings could be added as required. Future versions could have the photodiodes around the perimeter of the substrate with the electronics in the center allowing the LC deposited on top to effectively cover the entire chip area.

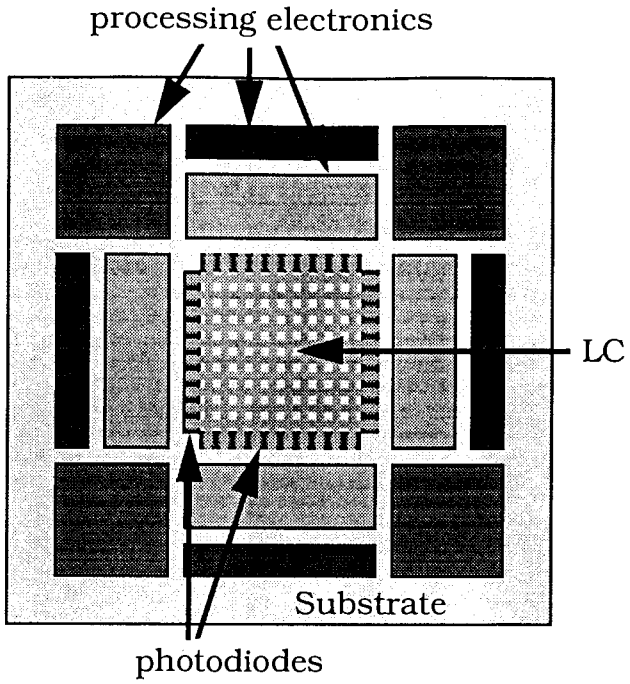

Figure 5.1 Integrated Scale Receptive Field System

Additional components used to construct the artificial eye which have been developed are a variable focus lens and an adaptive filter. To focus images at variable distances onto the LC would require some lens system. However, borrowing from the characteristics of the lens in the human eye, a system using a liquid filled lens built from an elastic film has been developed (Rawicz and Mikhailenko 1996) could eliminate the need for a bulky and complicated system using solid lenses. The current dynamic range of this LC based system is still not as good as that of the human visual system which uses several adaptation mechanisms and a retina with two receptor types (rods and cones) to allow for low and high illumination levels. To bring the dynamic range of the RFS closer to that of the human visual system, photochromic adaptive filters could be used, which have been developed to allow both local and global adaptation to

temporal and spatial light intensity variations (Wysokinski, Rawicz and Letowski 1995).

5.4 Other Applications

Although the artificial eye project was the primary motivation and rationale for some of the design constraints for the receptive field system, there are many other conceivable applications which could make use of such a system.

Laser Positioning and Tracking System

With very little modification, the RFS could form a significant portion of a laser positioning or tracking system. Generally, lasers produce intense, collimated, monochromatic beams of light. The RFS could easily track the motion of a laser spot if the LC it used had the peak absorption matched to the wavelength of the laser light. The light would be of sufficient intensity as to make any other background light insignificant to the RFS. Laser positioning systems can find uses in a large number of robotic automation facilities and the RFS would be a very simple, inexpensive and robust way of implementing them.

Smart Security Sensor

Current security sensors (not including camera based systems) typically work the following way. A beam of infrared radiation is projected and anything moving into the beam reflects a portion of it back which is detected, causing a security light or alarm to activate. One problem with

this is that the size and shape of the 'intruder' is irrelevant, and if used outside, a small animal can set it off causing a false alarm. The RFS could be adapted to function as a 'smart' security sensor. It would be capable of discriminating the color and angular dimensions of anything entering its field of view, thus eliminating false triggering.

Colorimetry

Colorimetric and spectral analysis of objects is generally performed using some kind of non-selective detector and a number of narrowband filters. Either the filters are sequentially moved in-between the detector and the object, or else the filters are fixed overtop of a number of similar detectors and this entire unit needs to be scanned across the object. Either way, the system or measurement is more complicated, and hence less reliable, than is necessary. By stacking multiple LCs in the RFS, each with a different spectral absorption characteristic, colorimetric measurements could be easily executed.

Appendix

A1 LC Fabrication

In the following Table A.1* is the base resin formulation for the UV curable polymer used to construct all the LCs discussed in this work. To this base formulation, the fluorescent dyes were added in the concentrations [%wt] mentioned earlier in the thesis. The concentration of Irgacure 184 added depended on the concentration and type of the fluorescent dye used.

Resin:	Constituent:	Chemical Composition:	Density: (g/mL)	%wt
UV1	Ebecryl 600	Epoxy diacrylate	1.202	60.0
	OTA 480	Propoxylated glycerol triacrylate	1.084	40.0
	Irgacure 184	1-Hydroxycyclohexyl phenyl ketone		~0.5

Table A.1 UV Curable Polymer

This polymer formulation allowed for patterning and curing in a single step using a close proximity negative mask of the desired layout and a high pressure mercury arc lamp.

---

* Ebecryl 600 and OTA 480 were obtained from UCB Radcure Incorporated, 131 Revco Road, North Augusta, South Carolina 29841. Igracure 184 was obtained from Ciba-Geigy Canada Limited, P.O. Box 2000, 7030 Century Avenue, Mississauga, Ontario L5M 5N3.

Fabrication Procedure

The following was adapted from a well established procedure known to result in uniform layers using a similar photopolymer resin formulation (Evenson and Rawicz 1995).

1. Clean: Rinse the glass slide in acetone as a mild degreasing step and spin dry (4000 rpm for 30 s).
2. Spin: Dispense polymer solution, spin (300 rpm 6x30 s) and allow wet film to settle for several minutes (~10 min.) to minimize bubble formation and to allow the self-leveling nature of the solution to produce a more uniform film.
3. UV Cure: Cure under a 100-W high-pressure Hg arc lamp in N_2 (for ~5 min.).
4. Develop: Rinse in acetone to remove uncured polymer and allow to dry.

The resulting films were uniform and their thickness measured with a micrometer was found to be 110 +/- 10 μm.

A2.1 Electronic Hardware

Components List

The following is a list of the essential electrical components used for the construction of the analog processing and control circuitry for the RFS which was explained in Chapter 3.

- TL054 Enhanced JFET Precision Quad Operational Amplifiers
- MC14066 Quad Analog Switches
- HCF4051 1 0f 8 Analog Multiplexers
- Sharp BS100C Photodiodes for Visible Light
- Motorola 68HC16 Microprocessor
- Resistors 5.1 MΩ
- Capacitors 0.1μF

Photodiode Characteristics

The following figures show the response characteristics of the photodiodes which were used in the RFS. Figure A.1 illustrates the photodiodes' spectral response while Figure A.2 shows the dynamic range of the photodiodes measured at 618 nm (the experimental peak). Finally, Figure A.3 indicates the RFS response as a function of the total power detected by all the photodiodes (measured @ 618 nm).

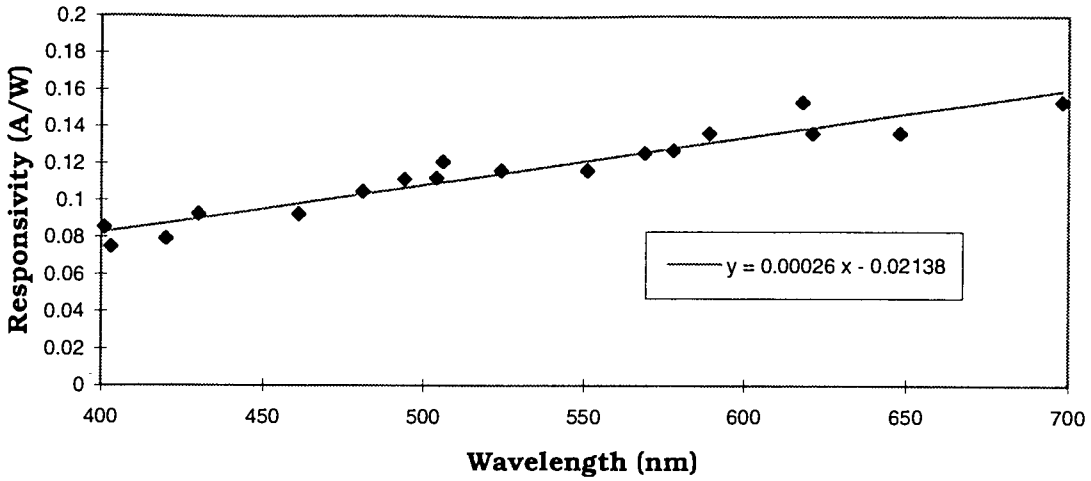

Figure A.1 Photodiode Spectral Response

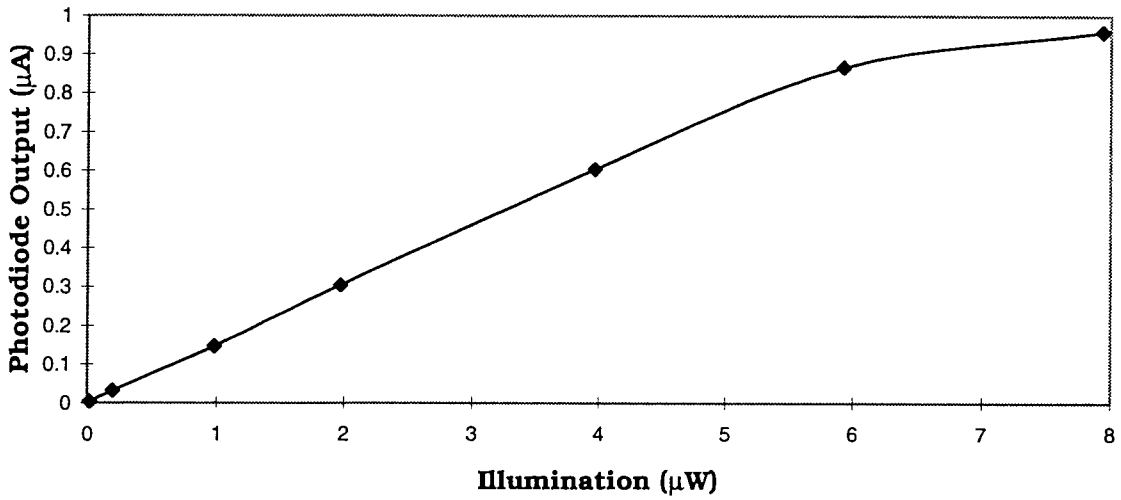

Figure A.2 Photodiode Responsivity

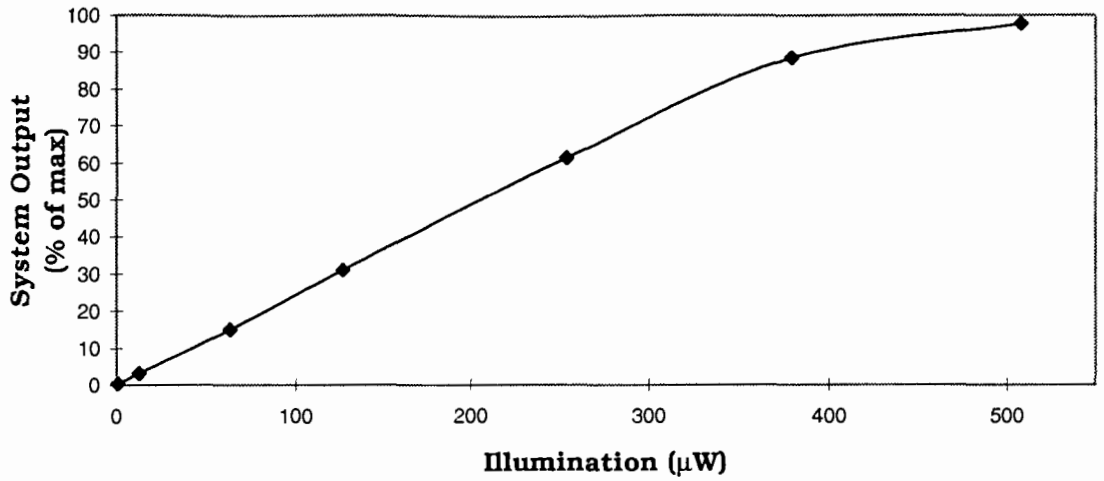

Figure A.3 RFS Photodiode Response

The photodiodes were 5.9 mm x 5.0 mm which limited the number which could be attached to an LC less than 10 cm across to 16. The active area was 1.55 mm^2 which determined the dimensions of the gridlines and channels on the LCs.

A2.2 Block Circuit Schematics

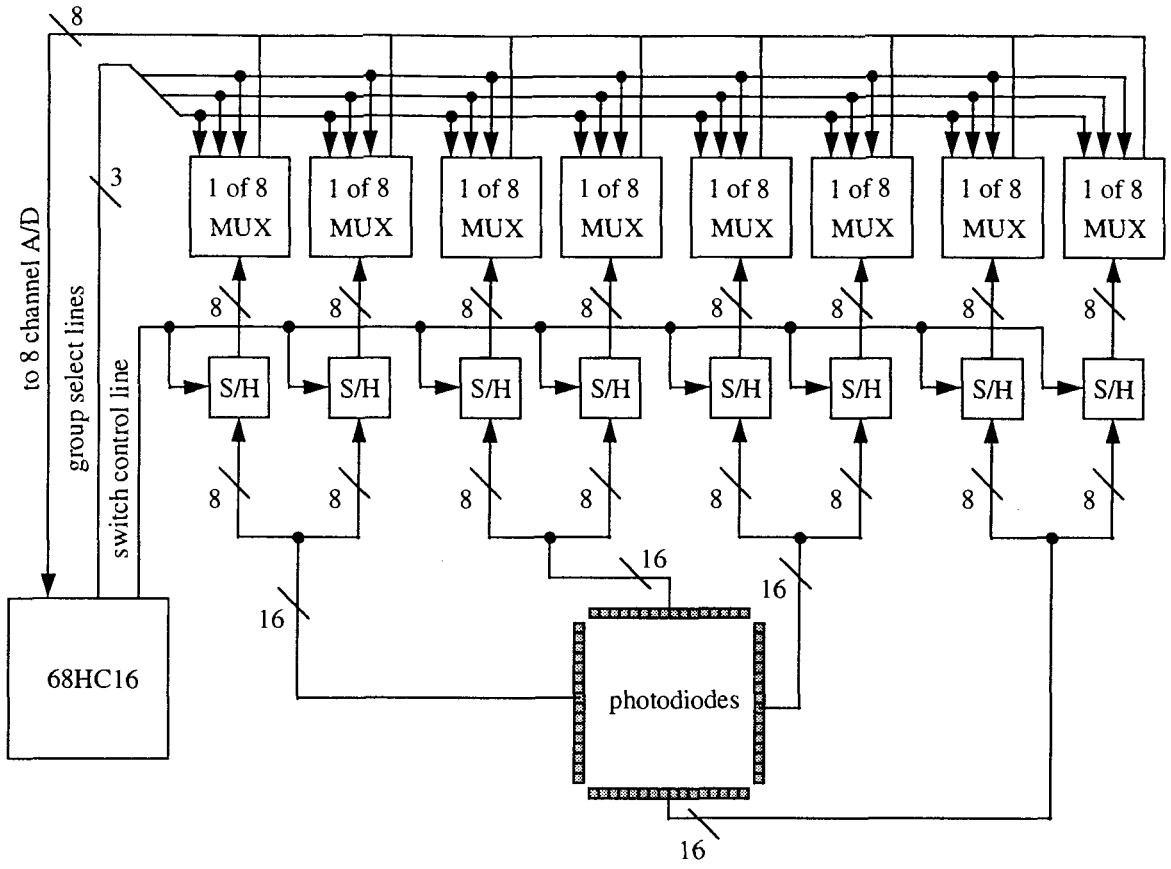

Figure A.4 RFS Block Circuit Schematic

A3 Assembly Code

The following is the complete assembly code written for the 68HC16 to interface to the hardware stage of the RFS system and the PC. It provides the control signals for the sample and hold, and multiplexing circuitry, collects the analog signals, converts them to digital values, and transmits them serially to the PC for further processing and analysis.

```
*************************************************************************
INCLUDE 'EQUATES.ASM'   ;table of EQUates for common register addresses
INCLUDE 'ORG00000.ASM'  ;initialize reset vector
INCLUDE 'ORG00008.ASM'  ;initialize interrupt vectors

MEMBANK         equ  $01      memory bank 1 designated for storage
A2DRESULTS      equ  $0000    memory location of first A/D conversion result
LASTRESULT      equ  A2DRESULTS+$80    location of last result
TEMP            equ  LASTRESULT+$02

ORG    $0200        ;start program after interrupt vectors
***** Initialization Routines *****
INCLUDE      'INITSYS.ASM'     ;initially set EK=F, XK=0, YK=0, ZK=0
                               ;set sys clock at 16.78 MHz, disable COP
INCLUDE      'INITRAM.ASM'     ;turn on 1k internal SRAM at $10000
                               ;set stack in bank 1 (SK=1, SP=03FE)
*I/O bank
     ldab   #$0F          set XK extension field to point to bank F
     tbxk
```

```
*ADC initialization
        ldd     #$0000          ADC power up (clears stop bit)
        std     ADCMCR
        ldd     #$00A3          10-bit resolution, 4 ADC clock period 'final
        std     ADCTL0          sample time', ADC clock = system clock/8

*GPT initialization
        ldd     #$0000          Set unrestricted access, and no interrupts
        std     GPTMCR
        ldab    #$FF            All input/output capture pins defined as
        stab    PDDR            outputs

*Serial interface initialization
        ldd     #$0037
        std     SCCR0           set the SCI baud rate to 9600 baud

        ldd     #$0008
        std     SCCR1           enable the SCI transmitter


***** Start of main program *****
MAIN:
        ldx     #GPTPDR
        ldab    #MEMBANK        set YK extension field to point to the RAM block
        tbyk
        ldab    #$08            SAMPLE
        stab    0,x
```

```
MAINLOOP:
        ldy    #A2DRESULTS
        ldab   #$00            Select group 1 sensors
        stab   0,x             HOLD

A2D_SAVE:
        jsr    A2D             do A/D conversion on analog inputs

        incb                   increment group#
        stab   0,x             multiplex next group of sensor inputs (note:
*                              if (B)=8, this also executes SAMPLE)
        bitb   #$08            reached 8th group of sensors yet?
        beq    A2D_SAVE        if not repeat, otherwise

        ldab   #$42            send a 'B' to indicate start of
        jsr    TCHAR           data block transmission
        ldy    #A2DRESULTS     store address of 1st A/D result

OUTPUT: ldd    0,y             get an A/D result to output
        jsr    SERIALOUT       output current A2D result serially
        aiy    #$02            increment location counter for the next result
        cpy    #LASTRESULT     output all 64 results yet?
        bne    OUTPUT          if not repeat, otherwise
        ldab   #$62            send a 'b' to indicate end of
        jsr    TCHAR           data block transmission
        bra    MAINLOOP        repeat forever
```

```
*******************************************************************************
*       A/D and Store Subroutine:  performs 10-bit A/D conversion on signals
*       at analog inputs AN0-AN7 and stores the results in memory
A2D:    pshb

        ldab    #$0F
        tbzk
        ldd     #$0030          8 channel (AN0-AN7), single conversions
        std     ADCTL1          - initiate
        ldz     #RJURR0         get address of right justified unsigned
*                               result registers
        ldaa    #$80
A2D_loop:
        bita    ADSTAT          conversion sequence complete?
        beq     A2D_loop        if not keep checking, otherwise

        ldaa    #$08            initialize save loop counter
SAVE_loop:
        lde     0,z             get A2D result
        ste     0,y             store it in memory
        aiz     #$02            point to next A2D result register
        aiy     #$02            point to next memory location
        deca                    all 8 results saved?
        bne     SAVE_loop       if not repeat, otherwise

        pulb
        rts                     return to main program
```

```
*******************************************************************************
*       Transmit Character Subroutine: Takes a byte stored in accumulator B
*       and outputs it serially to a P.C.
TCHAR:  ldaa    SCSR        read SCI status reg to check/clear TDRE bit
        anda    #$01        check only the TDRE flag bit
        beq     SERIALOUT   if TDR is not empty, go back to check it again
        ldaa    #$00        clear A to send a full word to SCDR ($FFC0E)
        std     SCDR        transmit one ASCII character to the screen

TC_LOOP:
        ldab    SCSR+1
        andb    #$80        test the TC bit (transfer complete)
        beq     TC_LOOP     continue to wait until TC is set

        rts
*******************************************************************************
*       Serial Output Routine:  Takes a binary number in accumulator D,
*       converts it to ASCII, and outputs it to the serial port.
SERIALOUT:
        pshm    x           push IX register
        lde     #$00        initialize loop counter

S_loop: ldx     #$0A        divide number by 10 for the
        idiv                BCD digit (from the remainder)

        addb    #$30        convert it to ASCII
        pshb                store the digit on the stack
```

```
        xgdx                put the quotient into D
        adde   #$01         increment loop counter
        cpe    #$05         looped 5 times?
        bne    S_loop       if not repeat, otherwise

        lde    #$00         initialize loop counter again
O_loop:
        pulb                Get digit from stack
        jsr    TCHAR        Output digit serially
        adde   #$01         increment loop counter
        cpe    #$05         output all 5 digits=1 A/D result
        bne    O_loop
        pulm   x            restore IX register
        rts
***** Exceptions/Interrupts *****

BDM:    bgnd                exception vectors point here
*                           and put the user in background mode
*
```

A4 Software functions - C code

The following is the complete listing of the code for the program used for interfacing to the RFS and displaying on screen numerically its output for given incident lighting conditions.

```
//*************************************************************************
// Program:    RFS Output
//
// Description: This program accepts A/D data from the serial port sent
//              from the 68HC16 board which is connected to the RFS.
//              This is then processed and used to plot the centroid of
//              the light pattern incident on the grid, which is done
//              continously, so that the motion of the light source can
//              be seen.  In addition, for testing purposes, the total
//              of all the photodiode voltage signals is output.
//*************************************************************************
#include <stdlib.h>
#include <stdio.h>
#include <graphics.h>
#include <conio.h>
#include <dos.h>
#include <math.h>
#include "serial.h"

#define      EVER  ;;
#define      xorg   192
```

```
#define     yorg   110
#define     gridw  15          // spacing between adjacent lines on grid LC
#define     gridcolor     12   // light red
#define     lightcolor    15   // white
#define     clip          0    // don't clip the drawings.
#define     SPOT_SIZE 2

void main()
{
        // request autodetection
        int gdriver = DETECT, gmode, errorcode;
        void *spot;
        int x, y, maxx, maxy, oldx, oldy, dx, dy, x_center, y_center;
        unsigned int size;
        int i, j, k, b, z, number, a2d_result=0, data_ok, port, port_ok;
        float x_sum, x_wsum, y_sum, y_wsum, x_volt, y_volt, volt1_sum,
              volt2_sum;
        int xsensor[17], ysensor[17], temp[64];
        int usensor[17], vsensor[17];
        unsigned char byte, path[30], buffer[250], port_number[2], string1[80],
                     string2[80];

        // Function prototypes
        void draw_grid();
        void draw_spot(int x, int y);
        void printvalues( unsigned char string1[80], unsigned char string2[80] );
```

```
// Initialize graphics and local variables
printf("\nEnter path for graphics driver\n");
gets(path);
initgraph(&gdriver, &gmode, path);
port_ok = 0;
while( !port_ok )
{
        printf("Enter serial port number (1 = COM1, 2 = COM2)\n");
        gets(port_number);
        if( atoi(port_number) == 1 )
        {
                port = COM1;
                port_ok = 1;
        }
        else if( atoi(port_number) == 2 )
        {
                port = COM2;
                port_ok = 1;
        }
        else
        {
                printf("Invalid choice\n");
                exit(0);
        }
}

// read result of initialization
```

```
errorcode = graphresult();
if (errorcode != grOk) { // an error occurred
        printf("Graphics error: %s\n", grapherrormsg(errorcode));
        printf("Press any key to halt:");
        getch();
        exit(1);
}
printf("Graphics mode = %s\n",getmodename(getgraphmode()));
printf("Max mode = %i\n",getmaxmode());

cleardevice();
setviewport( xorg, yorg, xorg+256, yorg+256, clip );
draw_grid();
setcolor( lightcolor );
x = 100;
y = 100;
draw_spot( x, y );

// calculate the size of the image and allocate space for it
size = imagesize(  x-SPOT_SIZE, y-SPOT_SIZE, x+SPOT_SIZE,
                   y+SPOT_SIZE );
spot = malloc(size);

// grab the image
getimage( x-SPOT_SIZE, y-SPOT_SIZE, x+SPOT_SIZE, y+SPOT_SIZE,
          spot);
oldx = x;
```

```
        oldy = y;

        init_serial( port, BAUD_9600, DATA_BITS_8, STOP_BITS_1,NO_PARITY );
//****** MAIN LOOP ****************************
        while( !kbhit() )
        {
                j = 1;
                k = 0;
                do // Check for start of data block transmission indicator
                        com_read_byte( port, &byte );
                while( byte != 'B' );

                // get the A2D data from the serial port and manipulate it
                for( EVER )
                {
                        com_read_byte( port, &byte );
                        if( byte == 'R' )
                        {
                                data_ok = 1;
                                continue;
                        }
                        if( byte == 'b' )  // check for end of block
                                break;
                        number = byte - '0';
                        a2d_result = 10 * a2d_result + number;
                        if( j>4 )
                        {//  Concatenate the 5 digit ASCII a2d results received
```

```
            // serially, convert them to integers and save them in
            // a temporary array.
                temp[k] = a2d_result;
                ++k;
                j=1;
                a2d_result = 0;
                data_ok = 0;
        }
        else ++j;
        if( kbhit() ) break;
}

for( j=0; j<8; ++j )    // Sort A2D results which are
{                       // received nonsequentially
        for( i=8*j,k=j; i<(2+8*j); ++i,k+=8 )
        {
                xsensor[16-k] = temp[i];
                ysensor[k+1] = temp[i+2];
                usensor[k+1] = temp[i+4];
                vsensor[16-k] = temp[i+6];
        }
}
// calculate the centroid of the light pattern
x_sum=x_wsum=y_sum=y_wsum=0;
for( i=1; i<17; ++i )
{
        x_sum += xsensor[i];
```

```
        x_wsum += i*xsensor[i];
        y_sum += ysensor[i];
        y_wsum += i*ysensor[i];
}

// sum the dc voltages for photodiode sets XY and UV
x_volt = x_sum*5.0/1023;
y_volt = y_sum*5.0/1023;
volt1_sum = x_volt + y_volt;
u_volt = u_sum*5.0/1023;
v_volt = v_sum*5.0/1023;
volt2_sum = u_volt + v_volt;

sprintf( string1, "X = %.2f, Y = %.2f, Total = %.2f",
          x_volt,y_volt,volt1_sum);
sprintf( string2, "U = %.2f, V = %.2f, Total = %.2f",
          u_volt,v_volt,volt2_sum);
printvalues( string1, string2 );

if( x_sum==0 )
{
        x_sum=1;
        x_wsum=8;
}
if( y_sum==0 )
{
        y_sum=1;
```

```
                y_wsum=8;
        }
        x_center = gridw * x_wsum / x_sum;
        y_center = gridw * y_wsum / y_sum;
        dx = x_center - oldx;
        dy = y_center - oldy;

        // erase old image
        putimage( oldx-SPOT_SIZE, oldy-SPOT_SIZE, spot, XOR_PUT );
        oldx += dx;
        oldy += dy;
        if( oldx > 256 )
                oldx = 256;
        if( oldy > 256 )
                oldy = 256;
        if( oldx < 0 )
                oldx = 0;
        if( oldy < 0 )
                oldy = 0;

        // plot new image
        putimage( oldx-SPOT_SIZE, oldy-SPOT_SIZE, spot, XOR_PUT);
}
// clean up
getch();
free(spot);
closegraph();
```

```
}
// USER DEFINED FUNCTIONS
void draw_spot(int x, int y)
{
        circle( x, y, SPOT_SIZE );
        floodfill( x, y, lightcolor);
}
void draw_grid()
{
        int x, y;
        setcolor( gridcolor );
        moveto( 0, 0 );
        for( x=gridw; x<250; x+=gridw )
        {
                moveto( x, 0 );
                lineto( x, 255 );
        }
        moveto( 0, 0 );
        for( y=gridw; y<250; y+=gridw )
        {
                moveto( 0, y );
                lineto( 255, y );
        }
}
void printvalues( unsigned char string1[80], unsigned char string2[80] )
{
        setcolor( lightcolor );
```

```
        setviewport( 0, 0, 400, 20, clip );  //setup new viewport for text
        clearviewport();
        outtextxy( 0, 0, string1 );          // output the current string
        setviewport( 0, 40, 400, 60, clip );  //setup new viewport for text
        clearviewport();
        outtextxy( 0, 0, string2 );          // output the current string
        // return to old viewport settings
        setviewport( xorg, yorg, xorg+256, yorg+256, clip );
}
//*****************************************************************************
```

By adding the following code segments, spatial and color processing of the incident light patterns was accomplished enabling the system to recognize size, shape, color and intensity gradients.

Nexus Calculation (Shape Determination)

```
//*****************************************************************************
            for( m=1; m<17; ++m )
            {
                    for( n=1; n<17; ++n )
                    {
                            p1 = x_sensor[m]*y_sensor[n];
                            p2 = x_sensor[m]*y_sensor[n];
                            p[m][n] =  p1/x_sum + p2/y_sum;
                            if( p[m][n] >= 1.0 )
                            {
                                    x = gridw*m;
```

```
                        y = gridw*n;
                        draw_spot( x, y );
                    }
                }
            }
```

Size and Gradient Calculation and Display

```
//*****************************************************************************
            {
                //erase old gradient and clear grid for next one
                setcolor( 0 );  //black
                for( i=1; i<5; ++i )
                {
                    ellipse( center_x, center_y, start_A, end_A, x_rad[i],
y_rad[i] );
                }
                setcolor( gridcolor );
                draw_grid();
            }
            setcolor( lightcolor );
            max_p = 1;
            max_px = max_py = 1;
            cx = cy = 1;
            light_found = 0;
            for( m=1; m<17; ++m ) //perform nexus calculation
            {
                for( n=1; n<17; ++n )
```

```
{
        p1 = x_sensor[m]*y_sensor[n];
        p2 = x_sensor[m]*y_sensor[n];
        p[m][n] =  p1/x_sum + p2/y_sum;
        // determine center for drawing concentric ellipses
        if( p[m][n] == max_p )
        {
                if( n == max_py )
                {
                        cx += 1;
                        tempx = 0;
                        for( i=0; i<cx; ++i )
                        {
                                tempx += m-i;
                        }
                        center_x = gridw*tempx/cx;
                }
                if( m == max_px )
                {
                        cy += 1;
                        tempy = 0;
                        for( i=0; i<cy; ++i )
                        {
                                tempy += n-i;
                        }
                        center_y = gridw*tempy/cy;
                }
```

```
                        }
                        if( p[m][n] > max_p )
                        {
                                max_p = p[m][n];
                                max_px = m;
                                max_py = n;
                                center_x = gridw * max_px;
                                center_y = gridw * max_py;
                        }
                }
        }

// Calculate gradients and display
if( light_found )
{
        draw_spot( center_x, center_y );
        for( i=1; i<5; ++i )                    //draw 4 concentric ellipses
        {                                       // with each one representing a
                p_temp = (1-(0.2*i))*max_p;     // 20% drop in intensity
                k = 1;
                for( j=1; j<(16-max_px); ++j )
                {
                        if( p_temp >= p[max_px+j][max_py] )
                        {
                                k = j;
                                break;
                        }
```

```
            }
            j = max( (k - 1), 0 );
            x_rad[i] = gridw*( k - ((p_temp - p[max_px+k][max_py])/max(
(p[max_px+j][max_py] - p[max_px+k][max_py]), 1 )) );
            k = 1;
            for( j=1; j<(16-max_py); ++j )
            {
                  if( p_temp >= p[max_px][max_py+j] )
                  {
                        k = j;
                        break;
                  }
            }
            j = max( (k - 1), 0 );
            y_rad[i] = gridw*( k - ((p_temp - p[max_px][max_py+k])/max(
(p[max_px][max_py+j] - p[max_px][max_py+k]), 1 )) );
            ellipse( center_x, center_y, start_A, end_A, x_rad[i], y_rad[i] );
      }
}
```

Color Extraction and Display

```
//*************************************************************************
//  Include this prior to the main loop of the RFS Output program
      getpalette(&pal);
      cleardevice();
      setrgbpalette(pal.colors[0], 0, 0, 0 );
      setrgbpalette(pal.colors[7], 50, 50, 50 );
```

```
        r = 32;
        g = 32;
        b = 0;
        spotcolor = 1;
        setrgbpalette(pal.colors[spotcolor], r, 0, 0 );//spot 1 initially red
//      setrgbpalette(pal.colors[2], 0, g, 0 );//spot 2 initially green
        draw_grid();
        x = 300;
        y = 100;
        draw_spot( x, y, 1 );
/*      u = 300;
        v = 200;
        draw_spot( u, v, 2 );
*/
        setcolor(7);
*****************************************************************************
// Add the following to the Main Loop after the data is received and sorted

// adjust color of light spots according to received intensity
red = r*(x_sum+y_sum)*2/1023;
green = g*(u_sum+v_sum)*2/1023;
x_volt = x_sum*5.0/1023;
y_volt = y_sum*5.0/1023;
u_volt = u_sum*5.0/1023;
v_volt = v_sum*5.0/1023;
setviewport( 0, 40, 400, 60, clip );  //setup new viewport for text
clearviewport();
```

```
sprintf( string, "X = %.2f, Y = %.2f, U = %.2f, V = %.2f", x_volt, y_volt, u_volt,
v_volt);
outtextxy( 0, 0, string );
setviewport( xorg, yorg, xorg+256, yorg+256, clip );// reset viewport
setrgbpalette(pal.colors[1], red, green, 0 );
//      setrgbpalette(pal.colors[2], 0, green, 0 );

if( user_input == 'm' ) // enter user controlled color modification loop
        {
                while( user_input != 'x'  )
                {
                        user_input = getch();
                        switch( user_input )
                        {
                                case 'q': // quit
                                {
                                        free(spot1);
//                                      free(spot2);
                                        closegraph();
                                        exit(1);
                                }
                                case 'r': if( r<63 ) r++; break;
                                case 'e': if( r>1 ) r--; break;
                                case 'g': if( g<63 ) g++; break;
                                case 'f': if( g>1 ) g--; break;
                                case 'b': if( b<63 ) b++; break;
                                case 'v': if( b>1 ) b--; break;
```

```
                        case '1': spotcolor = 1; break;
//                      case '2': spotcolor = 2; break;
                    }
                    if( spotcolor == 1 )
                    {
                        setviewport( 0, 0, 300, 20, clip );  //setup new
                                                             //viewport for text
                        clearviewport();
                        sprintf( string, "r=%i, red=%i, g=%i, green=%i", r,
red, g, green);
                        outtextxy( 0, 0, string );
                    }
                    if( spotcolor == 2 )
                    {
                        setviewport( 0, 40, 300, 60, clip ); //setup new
                                                             //viewport for text
                        clearviewport();
                        sprintf( string, "Spot 2: g=%i, green=%i",g,green);
                        outtextxy( 0, 0, string );
                    }
                }
                setviewport( xorg, yorg, xorg+256, yorg+256, clip );// reset
                                                                    //viewport
        }
}
```

```
// Replace the previous draw_spot function with this
void draw_spot(int x, int y, int spotcolor )
{
        setcolor( spotcolor );
        circle( x, y, SPOT_SIZE );
        setfillstyle( SOLID_FILL, spotcolor );
        floodfill( x, y, spotcolor);
}
```

A5 System Testing Procedures

The Receptive Field System was tested in ways which would allow determination of the system response as a whole. Additionally, it allowed for optimization of different configurations of LCs. The general setup and procedure used for testing is described below.

Setup

The entire receptive field system was placed on an optical bench in a dark room. Under these conditions, it was possible to stimulate the system with as much or as little light as was required for the various tests. The light source used was a tungsten filament projector with a focusing lens and variable power supply which allowed it to be calibrated to the 1931 CIE standard Illuminant A with a color temperature of 2850 K. It was placed on a rolling table which could be freely raised or lowered and moved closer or further away from the RFS. The detector portion of the RFS was set on edge so that it could be uniformly illuminated by the horizontal beam of light from the projector.

The light was assumed to be spatially uniform in intensity. However, the area illuminated was slightly larger than the area of the LC and masks were used directly in front of the LC to illuminate it with a pattern of the desired shape and size, rather than use lenses to focus the beam to the desired size. This way, if the light was not spatially uniform, at least the influence on successive measurements was minimized.

Startup Procedure

1. Power up system and initiate interface software for appropriate output on computer screen.
2. Record system response for dark room initial conditions.
3. Turn on light source and position it appropriate distance from RFS (typically 0.5 m) with entire LC area illuminated.
4. Increase illumination level until maximum response from all photodiodes is achieved to ensure proper operation. (Each photodiode is capable of outputting analog voltage signals between 0.0 and 5.0 V, so each sensor set has a maximum output of 32 photodiodes x 5 volts/photodiode = 160 volts.)

Area Sensitivity Measurement

Masks and a mask holder were fashioned from black construction paper which, when placed in front of the LC connected to the RFS, effectively blocked all incident light from being detected. Square holes were cut in the masks to allow different sized areas of the LC to be illuminated. These ranged from 4 cm^2 to 81 cm^2 or 5% to 100% of the total LC area. The holes were cut so that the areas of illumination were equidistant from the edges of the LC.

1. Fix illumination at an appropriate level so that with the full area of the LC illuminated, the RFS gives a constant response within its dynamic range (100 volts was chosen for simplicity).

2. Place reduced area mask in front of the LC, and record RFS output.
3. Repeat 2. for all area masks.

Spectral Sensitivity Measurement

In order to measure the spectral sensitivity of the RFS, 18 Balzer interference filters were chosen which adequately covered the range of wavelengths from 400 to 700 nm. Using these, the white light from the projector was filtered and used to illuminate the full area of the LC or LCs connected to the RFS. A Newport Model 815 Digital Power Meter with an 818-SL Detector was used to keep the level of illumination constant at each wavelength.

1. Place filter in projector and calibrate Power Meter to match the filter wavelength. Adjust lamp voltage until the Power Meter reading is at the chosen constant level. A power level of 0.200 +\- 0.002 mW was chosen, but the detector area was 0.785 cm^2. So the intensity of light was 0.255 +\- 0.003 mW/cm^2, resulting in 20.6 mW striking the 81 cm^2 surface of the LC.
2. Reposition the projector so the LC is fully illuminated and record the RFS response. The LC and Power Meter detector head were the same distance from the light source and right beside each other so all that was required to illuminate one or the other was simply rotating the projector a few degrees. Thus

the intensity of light striking the detector surface and LC was assumed to be the same.

3. Repeat above steps for all 18 filters.

Absolute Threshold Measurement

Once the absorption peaks were determined for the LCs from the spectral sensitivity measurements, the dynamic range of the RFS at each of these wavelengths could be measured. Due to limitations of the light source, and the optical density of the filters used, the upper threshold for the RFS with any of the LCs was not conclusively reached.

1. For a particular LC, place appropriate filter in projector.
2. Slowly increase the voltage for the light source until the RFS gives a reading just above that for the dark count. Record the power and the response as the lower threshold.
3. Increase the voltage for the light source, record the Power Meter reading and the RFS response for this setting.
4. Repeat 3. until the RFS response does not change when the illumination level is increased, or until the maximum illumination level is reached.

References

Batchelder, J., A. Zewail, and T. Cole (1979, September). Luminescent solar concentrators. 1: Theory of operation and techniques for performance evaluation. *Applied Optics 18*(18), 3090-3110.

Berlman, I. (1965). *Handbook of Fluorescence Spectra of Aromatic Molecules*. Academic Press, New York, New York.

Chamberlain, S. and J. Lee (1984, February). A Novel Wide Dynamic Range Silicon Photodetector and Linear Imaging Array. *IEEE Journal of Solid-State Circuits* 19 (1), 41-48.

Dennis, P. (1986). *Photodetectors: An Introduction to Current Technology.* Plenum Press, New York.

Dillon, P., A. Brault, J. Horak, E. Garcia, T. Martin, and W. Light (1976). Integral Color Filter Arrays For Solid State Imagers. *IEDM Technical Digest.*

Evenson, S. and A. Rawicz (1995, November). Thin-film luminescent concentrators for integrated devices. *Applied Optics 34*(31), 7231-7238.

Evenson, S. and A. Rawicz (1995, November). Thin-film luminescent concentrators for integrated devices: a cookbook. *Applied Optics 34*(31), 7302-7306.

Horowitz, P. and W. Hill (1980). *The Art of Electronics* (Second ed.). Cambridge University Press, Cambridge.

Le Grand, Y. (1968). *Light, Colour and Vision* (Second ed.). Chapman and Hall Ltd., London.

Leibovic, K. (Ed.) (1990). *Science of Vision.* Springer-Verlag New York Inc., New York, New York.

Rawicz, A. and I. Mikhailenko (1996, April). Modeling of a variable-focus liquid-filled optical lens. *Applied Optics 35*(10), 1587-1589.

Schäfer, F. (Ed.) (1977). *Dye Lasers* (Second ed.). Springer-Verlag New York Inc., New York, New York.

Tamir, T. (Ed.) (1988). *Guided-Wave Optoelectronics.* Springer-Verlag Berlin, Heidelberg.

Texas Instruments (1993). *Product Bulletin: CCD Area Array Image Sensors.* Texas Instruments, California.

Wandell, B. (1995). *Foundations of Vision.* Sinauer Associated, Inc., Sunderland, Massachusetts.

Wysokinski, T., A. Rawicz, and S. Letowski (1995, June). Modeling and Testing of a Light-Induced Spatial Light Modulator in Hybrid Optoelectronic Systems. *Microwave and Optical Technology Letters* 9(2), 72-77.